Pyrrolo[2,1-a]isoquinolines as multitasking organophotocatalysts in chemical synthesis

Liu, Yuliang

Li, Haoyu

Tan, Eugene Yew Kun

Santiko, Erik Budi

他

出版情報：Chem Catalysis. 2 (10), pp.2726-2749, 2022-10. Elsevier
バージョン：

Chem Catalysis

CellPress
OPEN ACCESS

Article

Pyrrolo[2,1-*a*]isoquinolines as multitasking organophotocatalysts in chemical synthesis

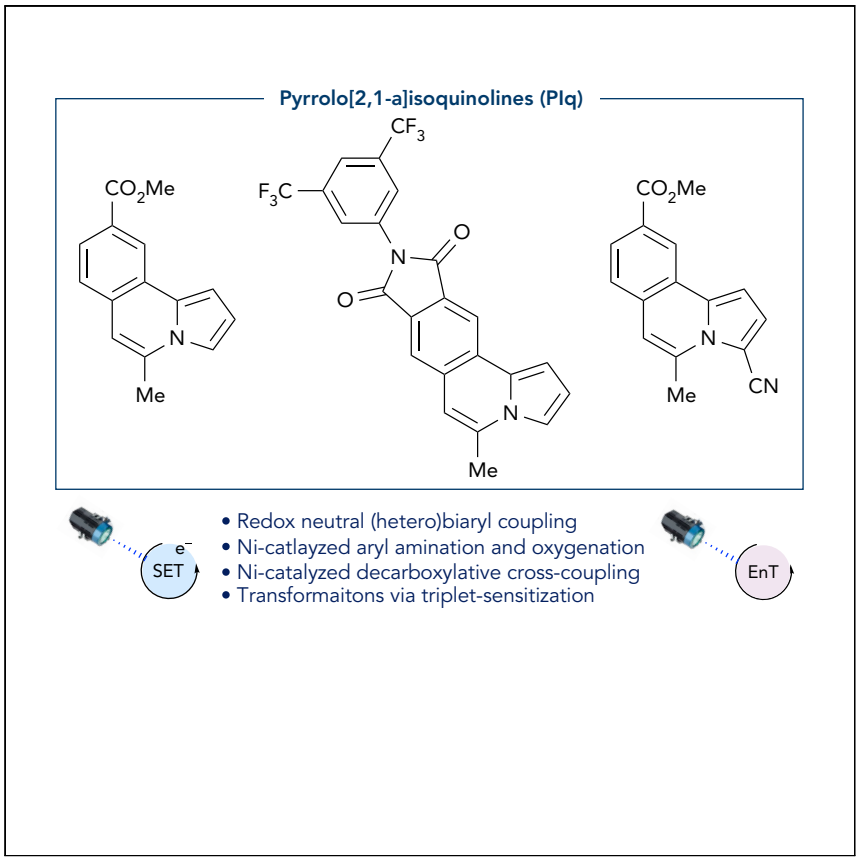

Chiba and co-workers have designed and developed pyrrolo[2,1-*a*]isoquinolines (PIqs) bearing electron-withdrawing groups as organic photocatalysts that display superior redox and energy-transfer functions to catalyze a series of molecular transformations.

Yuliang Liu, Haoyu Li, Eugene Yew Kun Tan, Erik Budi Santiko, Youhei Chitose, Manabu Abe, Shunsuke Chiba

mabe@hiroshima-u.ac.jp (M.A.)
shunsuke@ntu.edu.sg (S.C.)

Highlights

Pyrrolo[2,1-*a*]isoquinolines as a new scaffold of organophotocatalysts

Flexible tunability of PIqs on their photophysical and electrochemical characters

Multitasking capability of PIqs to catalyze a series of molecular transformations

Liu et al., Chem Catalysis 2, 2726–2749
October 20, 2022
Published by Elsevier Inc.
https://doi.org/10.1016/j.checat.2022.08.013

CellPress
OPEN ACCESS

Chem Catalysis

Article

Pyrrolo[2,1-*a*]isoquinolines as multitasking organophotocatalysts in chemical synthesis

Yuliang Liu,[1] Haoyu Li,[1] Eugene Yew Kun Tan,[1] Erik Budi Santiko,[2] Youhei Chitose,[2] Manabu Abe,[2,*] and Shunsuke Chiba[1,3,*]

SUMMARY

We demonstrate the design and synthesis of pyrrolo[2,1-*a*]isoquinolines (PIqs) bearing electron-withdrawing groups, which are excited under irradiation with visible light to display wider redox windows and higher triplet-state energies. The photophysical and electrochemical characters of PIqs can be tailored by modification of the electron-withdrawing groups and their positions, enabling redox-neutral (hetero)biaryl cross-coupling between aryl halides and (hetero)arenes, nickel-catalyzed amination and oxygenation of aryl halides, and decarboxylative cross-coupling between α-amino acids and aryl halides, as well as a set of molecular transformations driven by triplet-triplet sensitization under irradiation with visible light.

INTRODUCTION

Visible-light photocatalysis has been on the rise in advancing contemporary chemical synthesis in the last decade, enabling a vast array of molecular transformations.[1–6] Photocatalytic chemical processes are endowed with various chemical activation modes, including single-electron transfer (SET),[7,8] hydrogen-atom transfer (HAT),[9–11] and energy transfer (EnT),[12,13] as well as their combinations, which are generally induced by photoexcitation of light-absorbing substrates or complexes as the catalysts. Homogeneous transition-metal-based photocatalysts, such as ruthenium/iridium (Ru/Ir) polypyridyl complexes (e.g., **I**–**III** in Figure 1A), are employed as the photocatalysts, which can be excited under irradiation with visible light to form long-lived metal-to-ligand charge-transfer triplet excited states (^{3}MLCTs), inducing SET to or from organic substrates or EnT via triplet sensitization to provide reactive open-shell radical intermediates. To circumvent the use of transition metals given their rarity and toxicity, various organic photosensitizers have been designed and utilized as photocatalysts (Figure 1B).[14–16] Their basic structures commonly involve electron-donating groups (EDGs) and electron-withdrawing groups (EWGs) in π-conjugated scaffolds, and their appropriate spatial arrangement is key to enabling desired reactivities as the photocatalysts. The lifetimes of the excited singlet (S_1) states of organic photosensitizers are generally short (the decay rate constants k_d = ~10^{8-9} s^{-1}), whereas the rate constants of the intersystem crossing (ISC) to the triplet (T_1) state are about k_{ISC} = 10^{6-7} s^{-1}, except for those of molecules with heavy atoms or those of aryl ketones such as benzophenone derivatives with a close energy relation between $S_1(n,\pi^*)$ and $T_1(\pi,\pi^*)$, thus resulting in relatively low quantum yields of ISC.[14,17] Therefore, long-lived T_1 states are not efficiently employed for the desired bimolecular electron-transfer or EnT events. 10-Phenyl-phenothiazine (PTH; **IV**)[18,19] and acridinium salts (e.g., **V**)[20] are known to function as a S_1 excited-state photoreductant and photooxidant, respectively.

THE BIGGER PICTURE

Visible-light photocatalysis, which harvests readily available visible photons to drive chemical processes, has unlocked new reactivity paradigms, leading to vast expansion of the chemical spaces for the production of small molecules of interest. In this work, we have designed and developed pyrrolo[2,1-*a*]isoquinolines (PIqs) bearing electron-withdrawing groups as organic photocatalysts that display superior redox and energy-transfer functions to catalyze a series of molecular transformations. The reactivity of PIqs can be precisely tuned by the positions and types of the electron-withdrawing groups on the compact PIq scaffold, guiding them to the desired photocatalysis of choice.

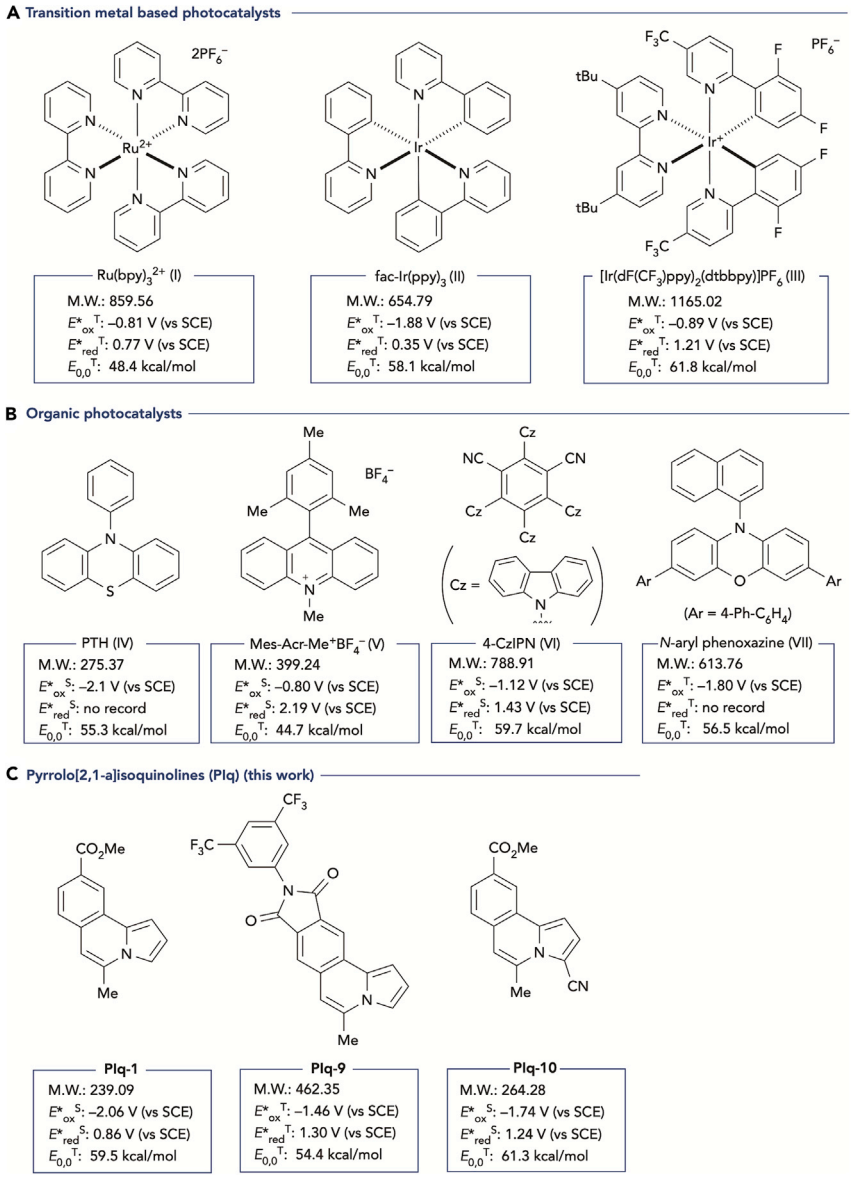

Figure 1. Photocatalysts

However, the lifetime of their S_1 states is short (τ = 3 ns for **IV** and 6 ns for **V**, k_d = ~1.5–3 × 10^8 s^{-1}), and thus the applicable reactions might be restricted to those at a near-diffusion limit (for example, ~2–5 × 10^9 $M^{-1}s^{-1}$ with the substrate concentration around at 0.1 M). On the other hand, a donor-acceptor cyanoarene, 1,2,3,5-tetrakis(carbazol-9-yl)-4,6-dicyanobenzene (4-CzIPN; **VI**), was identified by Adachi as an excellent thermally activated delayed fluorescence (TADF) material that has a small energy gap between the excited S_1 and T_1 states (ΔE(ST) = nearly 2 kcal mol^{-1}) and thus shows an extremely longer-lived photoluminescence lifetime (τ = ~5 μs, k_d = ~2 × 10^5 s^{-1}).[21–23] However, the redox window of photoexcited **VI** (E^*_{red} = 1.35 V versus saturated calomel electrode [SCE]; E^*_{ox} = −1.04 V versus SCE) is not so wide, and thus its catalysis application for the redox activation of small molecules is restricted.[24] Zeitler successfully expanded the photoexcited redox window of donor-acceptor cyanoarenes through structural fine-tuning of the electron-donor

[1]Division of Chemistry and Biological Chemistry, School of Physical and Mathematical Sciences, Nanyang Technological University, Singapore 637371, Singapore

[2]Department of Chemistry, Graduate School of Advanced Science and Engineering, Hiroshima University, Higashi-Hiroshima, Hiroshima 739-8526, Japan

[3]Lead contact

*Correspondence: mabe@hiroshima-u.ac.jp (M.A.), shunsuke@ntu.edu.sg (S.C.)

https://doi.org/10.1016/j.checat.2022.08.013

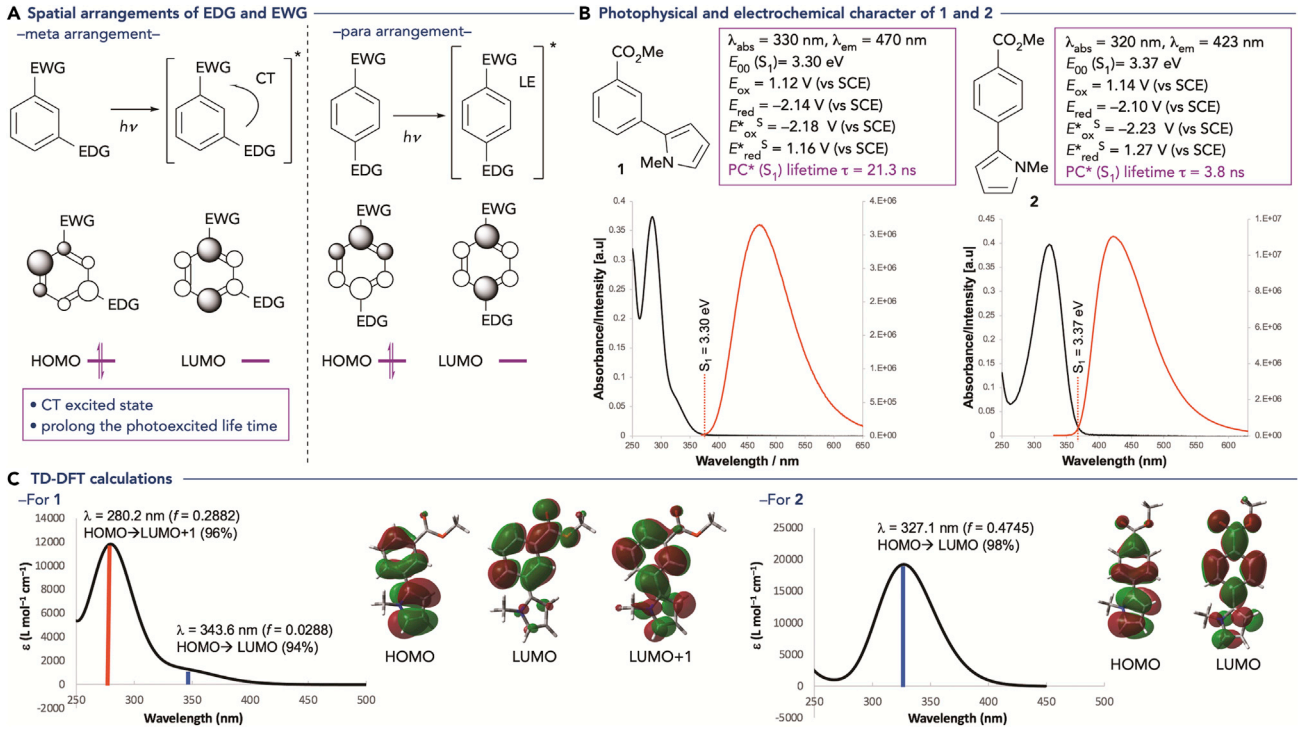

Figure 2. Photophysical and electrochemical characterization of 1 and 2

(A) Spatial arrangement of an EDG and an EWG on a benzene ring for photocatalyst design.

(B) Photophysical and electrochemical characters of methyl 3-(1-methyl-1*H*-pyrrol-2-yl)benzoate (**1**) and methyl 4-(1-methyl-1*H*-pyrrol-2-yl)benzoate (**2**). Some representative data are listed. Absorption (black line) and fluorescence emission (red line) spectra are shown for both **1** and **2** (see Figures S9–S14, S45, and S46).

(C) Absorption spectra of **1** and **2** with contributions of their frontier orbitals to the absorption peaks computed at the B3LYP/6-31G(d) level of theory (see Figures S60 and S61).

and -acceptor moieties, tailoring them for stronger photoexcited reductants (E^*_{ox} up to −1.79 V versus SCE) or oxidants (E^*_{red} = 1.56 V versus SCE).[25] Miyake developed a series of organic visible-light photocatalysts based on *N*-aryl phenoxazines (e.g., **VII**), which are capable of populating long-lived photoexcited T_1 states with highly negative oxidation potentials (E^*_{ox} = up to −2 V versus SCE) and higher quantum yields of their ISC, and thus these photocatalysts have been utilized as a photoexcited reductant to initiate the processes.[26–30] Their CT state involving orthogonally twisted donor and acceptor moieties is one of the keys to promoting ISC from S_1 to T_1 in higher yield.

Herein, we report that pyrrolo[2,1-*a*]isoquinolines (PIqs) bearing EWGs are capable of displaying a wider redox potential window and higher excitation energy in their photoexcited states to promote a set of SET and EnT events under irradiation with visible light, despite their planar and compact core scaffolds (Figure 1C). Interestingly, the position and the types of the EWGs on the PIq scaffold have a significant impact on their photophysical and electrochemical characters, such as the photoexcited states and their lifetimes, as well as electrochemical potentials and T_1 state energies. We discuss the rational design and development of PIqs, as well as their photocatalytic applications, to promote redox-neutral biaryl cross-coupling, nickel-catalyzed aryl amination and oxygenation, and decarboxylative cross-coupling, as well as a set of molecular transformations driven by triplet-triplet sensitization.

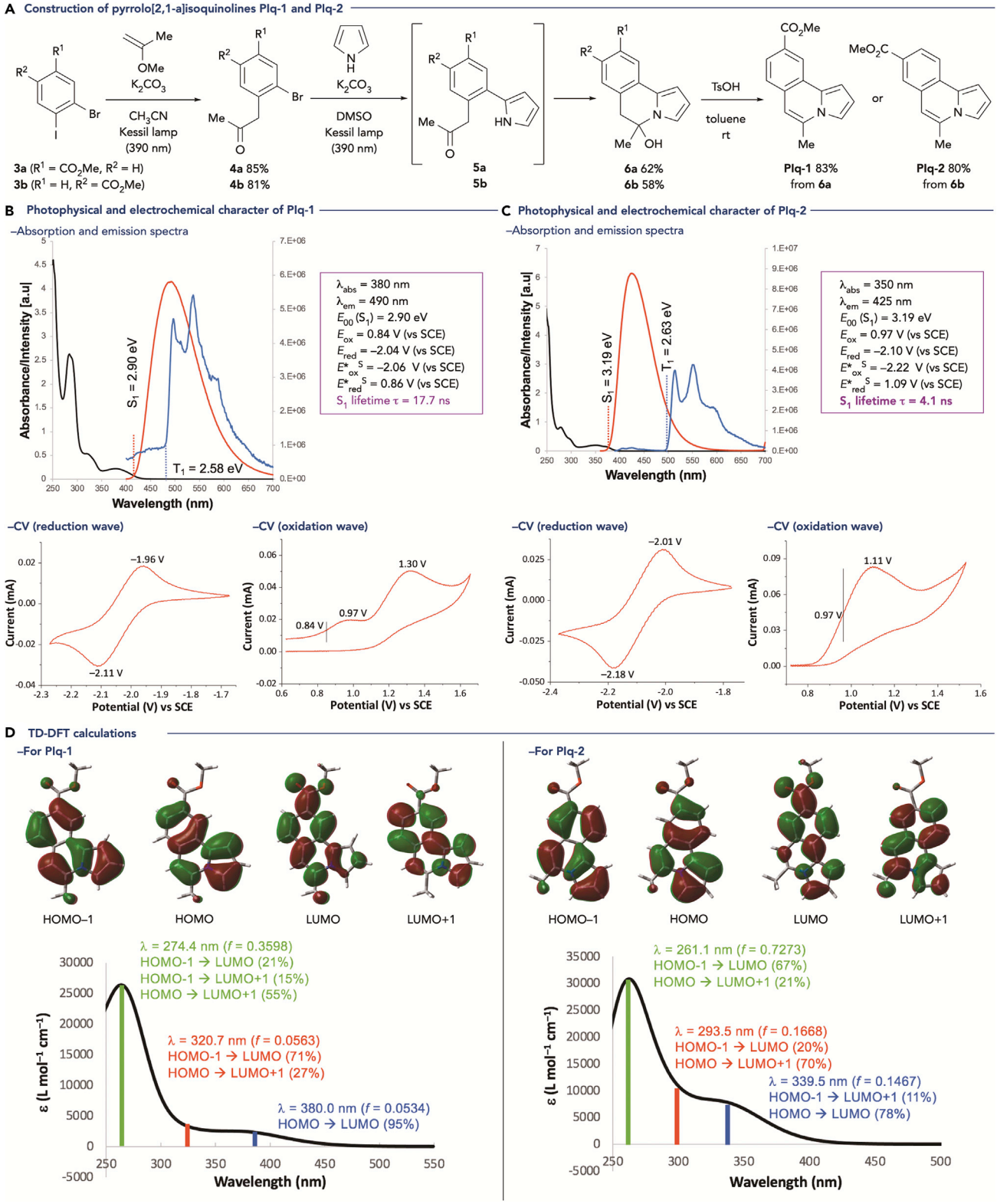

Figure 3. Synthesis of Plq-1 and Plq-2 and their photophysical and electrochemical characterization

(A) Synthesis of **Plq-1** and **Plq-2**.

Figure 3. *Continued*

(B) Photophysical and electrochemical characters of **PIq-1**. Some representative data are listed. Absorption (black line), fluorescence emission (red line), and phosphorescence emission (blue line) spectra are shown (see Figures S15–S17 and S47).

(C) Photophysical and electrochemical characters of **PIq-2**. Some representative data are listed. Absorption (black line), fluorescence emission (red line), and phosphorescence emission (blue line) spectra are shown (see Figures S18–S20 and S48).

(D) Absorption spectra of **PIq-1** and **PIq-2** with contributions (>10%) of their frontier orbitals to the absorption peaks computed at the B3LYP/6-31G(d) level of theory (see Figures S62 and S63).

RESULTS AND DISCUSSION

Design, synthesis, and characterization of PIqs

As a molecular design strategy, the spatial separation of EDG and EWG sites that are not directly conjugated within the π-conjugated scaffolds is essential to enabling an intramolecular charge transfer (CT) state, thus enabling a prolonged lifetime of the electronically excited states.[31] Thus, our design is based on the installation of EDG and EWG at the 1 and 3 positions of the benzene ring (Figure 2A). As for the electron-donating moieties, amino groups (–NR_2) have been conventionally employed and introduced by typically transition-metal-catalyzed aryl–N cross-coupling reactions or nucleophilic aromatic substitution reactions. On the other hand, we selected an electron-rich five-membered ring aromatic heterocycle, pyrrole,[32] as a candidate of the EDG and installed it through a C–C bond that allows for elongation of π-conjugate structures of the scaffolds. As a proof of concept, we first studied (2-pyrrolyl)benzoates (**1** for meta-adduct, **2** for para-adduct) (Figure 2B). A set of photophysical and electrochemical measurements revealed that they displayed reasonably wider redox potential windows in their photoexcited S_1 states (for **1**: $E^*_{ox}{}^S = -2.14$ V versus SCE, $E^*_{red}{}^S = 1.12$ V versus SCE; for **2**: $E^*_{ox}{}^S = -2.23$ V versus SCE, $E^*_{red}{}^S = 1.27$ V versus SCE). More interestingly, the meta-adduct **1** showed longer fluorescence lifetime of nearly 21 ns than that of the para-adduct **2** (3.8 ns) measured by time-correlated single photon counting (TCSPC). We also observed a larger Stokes shift ($\lambda_{abs.max} = 330$ nm, $\lambda_{em.max} = 470$ nm, $\Delta\lambda = 140$ nm), which indicates desired CT character of **1** in its photoexcited state.[33]

To shed light on the electronic transitions that are responsible for the absorption of **1** and **2**, we conducted time-dependent density functional theory (TD-DFT) calculations at the B3LYP/6-31G(d) level of theory (Figure 2C). It revealed that meta-adduct **1** has highest occupied molecular orbital (HOMO) and lowest unoccupied molecular orbital (LUMO) localized on the pyrrole and benzoate moieties, respectively, and thus the transition from HOMO to LUMO is characterized as the CT nature with predicted λ_{abs} at 344 nm and small oscillator strength (*f*) of 0.029, while its $\lambda_{max,abs}$ at 280 nm ($f = 0.29$) is assigned to be the transition from HOMO to LUMO +1 as the local excitation (LE) of the 2-arylpyrrole moiety. On the contrary, para-adduct **2** possesses its electronic transition from HOMO (π) to LUMO (π*) given that its $\lambda_{max,abs}$ is at 327 nm with a relatively large oscillator strength (*f*) of 0.47. These theoretical data corroborate the empirical observations (Figure 2B).

Further to endow them with a visible-light-absorbing character with greater molar absorptivity, elongation of the π-conjugated system was attempted by bridging the pyrrole nitrogen and the ortho-aromatic carbon with a C=C double bond. For this purpose, we adopted the photoinduced radical cross-coupling protocols under transition-metal-free manners originally developed in our group (Figure 3A). At first, we performed photoinduced acetomethylation of methyl 3-bromo-4-iodobenzoate (**3a**) with 2-methoxypropene, which proceeded selectively at the aryl-I bond to form **4a**.[34] Subsequently, photoinduced biaryl cross-coupling with pyrrole at the remaining bromide site of **4a** was conducted,[35] furnishing cyclic hemiaminal **6a** via spontaneous cyclization of the biaryl coupling product **5a**. Treatment of **6a** with TsOH induced dehydration,

Table 1. Photophysical and electrochemical characterization of PIqs

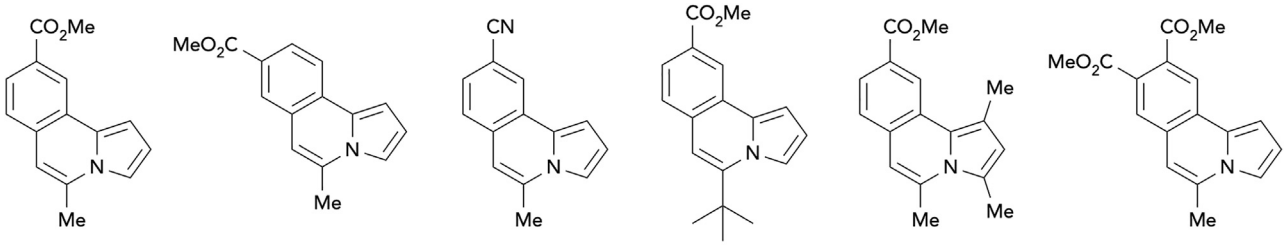

Entry	PIq	MW	$\lambda_{abs/em\ max}$ (nm)[a]	Φ (fl)[b]	τ (S_1) (ns)[c]	τ (T_1) (μs)[d]	$E_{0,0}$ (eV)[e]	E_{ox} (V)[f]	E_{red} (V)[f]	E^*_{ox} (V)[g]	E^*_{red} (V)[h]
1	**PIq-1**	239.09	380/490	0.41	17.7	104	2.90 (S_1), 2.58 (T_1)	0.84	−2.04	−2.06 (S_1), −1.74 (T_1)	0.86 (S_1), 0.54 (T_1)
2	**PIq-2**	239.09	350/425	0.54	4.1	95	3.19 (S_1), 2.63 (T_1)	0.97	−2.10	−2.22 (S_1), −1.66 (T_1)	1.09 (S_1), 0.53 (T_1)
3	**PIq-3**	206.25	375/475	0.40	16.5	τ_1: 4.6 (73%); τ_2: 153 (27%)	2.94 (S_1), 2.56 (T_1)	1.05	−2.04	−1.89 (S_1), −1.51 (T_1)	0.90 (S_1), 0.52 (T_1)
4	**PIq-4**	281.36	382/493	0.44	18.2	95	2.87 (S_1), 2.56 (T_1)	0.83	−2.00	−2.04 (S_1), −1.73 (T_1)	0.87 (S_1), 0.56 (T_1)
5	**PIq-5**	267.33	405/531	0.16	8.5	17	2.69 (S_1), 2.43 (T_1)	0.57	−2.08	−2.12 (S_1), −1.86 (T_1)	0.61 (S_1), 0.35 (T_1)
6	**PIq-6**	297.31	349/506	0.18	9.8	42	2.93 (S_1), 2.58 (T_1)	0.76	−1.90	−2.17 (S_1), −1.82 (T_1)	1.03 (S_1), 0.68 (T_1)

[a]The lowest energy absorption maxima and the highest energy fluorescence emission maxima measured in DMSO (see Figures S15, S18, S21, S24, S27, and S30).
[b]Fluorescence quantum yields.
[c]Lifetime of S_1 states determined by TCSPC (see Figures S16, S19, S22, S25, S28, and S31).
[d]Lifetime of T_1 states measured by transient absorption spectroscopy (see Figures S17, S20, S23, S26, S29, and S32).
[e]Excitation energies ($E_{0,0}$) for the S_1 and T_1 states. $E_{0,0}$ for S_1 were taken from the intersection of the absorption and fluorescence emission bands. $E_{0,0}$ for T_1 were estimated from the onset of the phosphorescence emission spectra.
[f]The electrochemical potentials (V versus SCE) measured by CV (see Figures S47–S52).
[g]Photoexcited oxidation potentials in S_1 and T_1 states calculated with $E_{0,0}$ and E_{ox}.
[h]Photoexcited reduction potentials in S_1 and T_1 states calculated with $E_{0,0}$ and E_{red}.

leading to the construction of 5-methylpyrrolo[2,1-*a*]isoquinoline carboxylate **PIq-1**, which is an analog of the meta-adduct **1**. By following the same protocols, we also prepared **PIq-2**, an analog of the para-adduct **2**, from 4-bromo-3-iodobenzoate (**3b**). As expected, **PIq-1** showed its absorption tailing to the visible spectral range ($\lambda_{abs,\ max}$ = 380 nm) with an excitation energy ($E_{0,0}^S$) of 2.90 eV, which was taken from the intersection of the absorption and fluorescence emission bands (Figure 3B). Despite its planar structure, we observed a relatively longer-lived fluorescence lifetime (18 ns) like for the meta-adduct **1**. In the cyclic voltammetry (CV) measurements of **PIq-1**, a quasi-reversible reduction wave was observed ($E_{red\ 1/2}$ = −2.04 V versus SCE), whereas the oxidation wave was irreversible ($E_{ox\ p/2}$ = 0.84 V versus SCE). These data indicated that **PIq-1** can function as a visible-light-absorbing photosensitizer with a wider redox window as a potent photoexcited reductant ($E^*_{ox}{}^S$ = −2.06 V versus SCE) and also as a mild photoexcited oxidant ($E^*_{red}{}^S$ = 0.86 V versus SCE) in its S_1 excited state. The phosphorescence emission spectrum of **PIq-1** was recorded in EtOH-2-methyltetrahydrofuran solution at 77 K under an argon atmosphere, revealing that **PIq-1** has relatively higher excited T_1 state energy ($E_{0,0}^T$) = 2.58 eV (59.5 kcal/mol). Therefore, we surmised that **PIq-1** might have a multitasking ability to take advantage of both S_1 and T_1 states for the photoinduced SET and EnT events, respectively. In turn, the photophysical and electrochemical characterization of **PIq-2** (Figure 3C) revealed that it possesses a similar redox profile to **PIq-1**, although its absorption is kept in the UVA region with a higher excitation energy ($E_{0,0}^S$) of 3.19 eV and a much shorter fluorescence lifetime (4 ns). TD-DFT calculations at the B3LYP/6-31G level of theory further supported these empirical data of **PIq-1** and **PIq-2** (Figure 3D). Similarly with meta-adduct **1** (Figure 2C), the red-shifted absorption at λ_{abs} = 380 nm of **PIq-1**

Table 2. Optimization of the reaction conditions for heterobiaryl cross-coupling

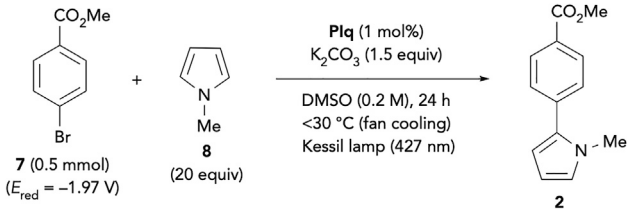

Entry	Plq	Conversion of 1 (%)[a]	Yield of 2 (%)[a]
1	**Plq-1**	>99	85 (81),[b] (83)[c]
2	no catalyst	13	<5
3	**Plq-3**	85	71
4	**Plq-4**	60	53
5	**Plq-5**	61	49
6	**Plq-6**	91	75

Reaction conditions: **7** (0.5 mmol), **8** (20 equiv), Plq (1 mol %), K_2CO_3 (1.5 equiv), DMSO (2.5 mL), 427 nm light (Kessil lamp), <30°C with fan cooling (see Figures S1 and S2).

[a]^{1}H NMR yields based on the internal standard.

[b]Isolated yield.

[c]Isolated yield from the reaction using 2.5 mmol of **7**.

was predicted with a relatively small oscillator strength (*f*) of 0.054 derived from the CT-like transition from HOMO (the pyrrole moiety) to LUMO (the benzoate moiety), whereas **Plq-2** showed the electronic transition from HOMO (π) to LUMO (π^*) observed at λ_{abs} = 340 nm with a relatively large oscillator strength (*f*) of 0.15. The relatively large oscillator strength for **Plq-2** can be explained by larger orbital overlapping of HOMO with LUMO in **Plq-2** than that in **Plq-1** (Figure 3D). The CT character of **Plq-1** in its S_1 state was proved by the significant solvatochromic effect[36] in the emission of **Plq-1** under irradiation with 360 nm light in solvents of different polarity (see Figures S57–S59). The fluorescence emission maxima of **Plq-1** were red shifted more significantly than those of **Plq-2** with increasing solvent polarity.

By following the synthetic protocol of **Plq-1** and **Plq-2** in Figure 3A, we also designed and synthesized several analogs, **Plq-3** to **Plq-6**, and conducted their photophysical and electrochemical characterization (Table 1). The replacement of a methoxycarbonyl group of **Plq-1** with a cyano group (**Plq-3**) made its reducing ability slightly lower ($E^*_{ox}{}^S$ = −1.89 V versus SCE) (entry 3), while installation of a *t*-butyl group in place of a methyl group (**Plq-4**) did not affect their photophysical or electrochemical characters (entry 4). Installation of methyl groups onto the pyrrole ring (**Plq-5**) made its fluorescence lifetime shorter without enhancing its reducing ability (entry 5). In turn, to enhance the oxidizing ability, we installed the second methoxy carbonyl group onto the arene moiety of the Plq scaffold. However, the resultant **Plq-6** showed moderate photoexcited reduction potential ($E^*_{red}{}^S$ = 1.03 V versus SCE) while keeping highly negative photoexcited oxidation potential ($E^*_{ox}{}^S$ = −2.17 V versus SCE) in its photoexcited S_1 state. Nonetheless, these data indicate that Plqs have relatively lower molecular weight (MW) and unique and outcompeting characters in redox and EnT capability in comparison with other known photocatalysts.

Application of Plqs to photocatalysis

Heterobiaryl cross-coupling

Given that Plqs are endowed with highly negative photoexcited oxidation potentials (E^*_{ox} < −2 V versus SCE, except for **Plq-3**), we surmised that they can potentially

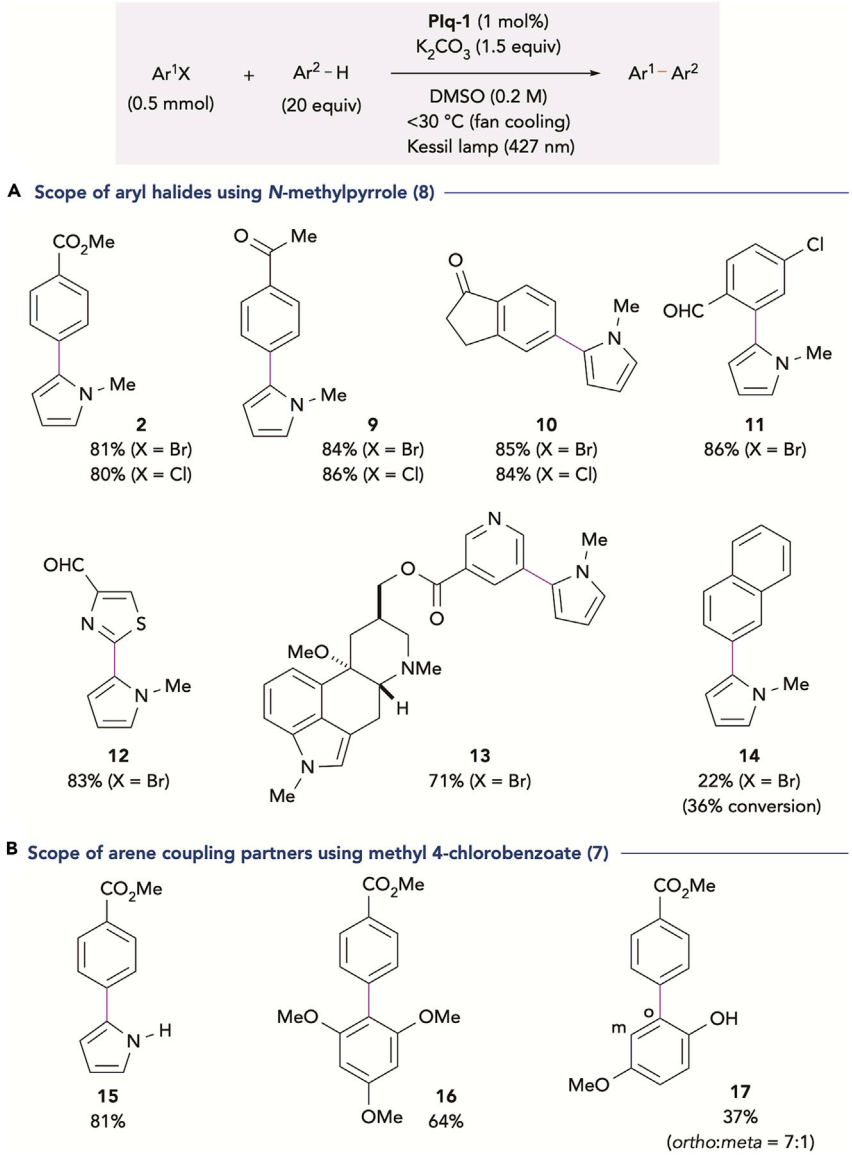

Figure 4. Substrate scope on heterobiaryl cross-coupling

work for reductive generation of aryl radicals from aryl halides.[37,38] To prove this hypothesis, we investigated a heterobiaryl cross-coupling reaction between methyl 4-bromobenzoate (**7**) (E_{red} = −1.97 V versus SCE) and *N*-methylpyrrole (**8**) as a benchmark (Tables 2 and S7).[34,39–43] We observed a smooth coupling reaction when the mixture of **7** and **8** (20 equiv) was treated with **PIq-1** (1 mol %) in the presence of K_2CO_3 (1.5 equiv) in DMSO under irradiation with 427 nm light, leading a full conversion of **7** to afford heterobiaryl **2** in 85% NMR yield (81% isolated yield) (entry 1). We confirmed that almost no background reaction took place in the absence of **PIq-1**, thus unambiguously indicating the capability of **PIq-1** as a photoredox catalyst.[44] We found that **PIq-3** to **PIq-6** were inferior to **PIq-1** in photoredox reactivity for the heterobiaryl cross-coupling (entries 3–6). We also confirmed that **PIq-1** could be recovered in more than 90% yield after the completion of the cross-coupling reaction (see the supplemental information for details).

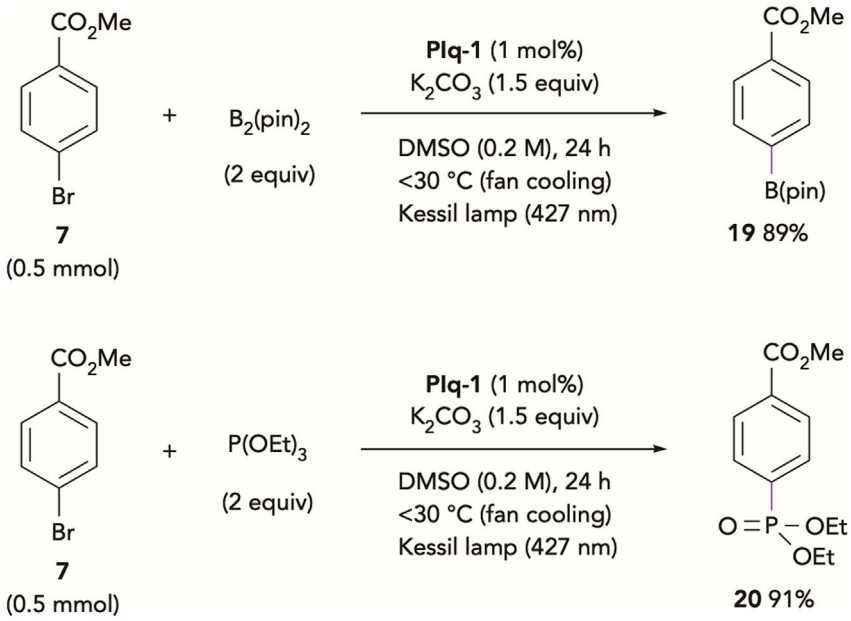

Figure 5. Borylation and phosphorylation of 7

We next investigated scope and limitation for the heterobiaryl cross-coupling using **PIq-1** as the photoredox catalyst under irradiation with 427 nm light (Figure 4). We found that the present photocatalytic system with **PIq-1** is able to engage not only aryl bromides but also less reactive aryl chlorides having an EWG to provide heterobiaryls **2**, **9**, and **10** in good yields. The reaction of 2-chloro-4-bromobenzaldehyde proceeded selectively at the bromide site to form **11** in 86% yield. The present catalytic protocol could successfully employ heteroaryl halides based on thiazole (for **12**) as well as pyridine (for **13** based on nicergoline). However, the reaction of 2-bromonaphthalene (E_{red} = −2.19 V versus SCE) became sluggish to form **14** only in 22% yield with incomplete conversion (36% conversion yield). This method could employ not only *N*-H pyrrole (for **15**) but also electron-rich arenes such as 1,3,5-trimethoxybenzene and 4-methoxyphenol as the arene coupling partner (for **16** and **17**).

Furthermore, this photocatalytic reductive functionalization of aryl halides could be extended to borylation with bis(pinacolato)diboron ($B_2(pin)_2$)[45–47] and phosphorylation with triethyl phosphite ($P(OEt)_3$) (Figure 5).[48]

We observed through TCSPC that the fluorescence lifetime ($^1\tau$ = 17.7 ns, ^1k_d = 5.65 × 10^7 s^{-1}) of **PIq-1** (60 mM, excitation at 390 nm, emission at 490 nm) was shortened in the presence of methyl 4-bromobenzoate (**7**) in DMSO under an argon atmosphere at 293 K (Figure 6A): $^1\tau$ = 17.7 ns with [**7**] = 0 mM, $^1\tau$ = 17.3 ns with [**7**] = 30 mM, $^1\tau$ = 17.1 ns with [**7**] = 50 mM, $^1\tau$ = 16.8 ns with [**7**] = 80 mM, $^1\tau$ = 16.6 ns with [**7**] = 100 mM, $^1\tau$ = 16.4 ns with [**7**] = 120 mM, $^1\tau$ = 16.2 ns with [**7**] = 150 mM, and $^1\tau$ = 15.7 ns with [**7**] = 200 mM. The Stern-Volmer plot indicated that the dynamic quenching rate constant (^1k_q) of the S_1 photoexcited state of **PIq-1** by **7** is 3.47 × 10^7 M^{-1} s^{-1} (Figure 6B). Similarly, 4-bromoacetophenone also quenched S_1 of **PIq-1** with a rate constant of 1.35 × 10^8 M^{-1} s^{-1} (see Table S10 and Figure S64).

We investigated the dynamic quenching of the T_1 state of **PIq-1** by **7** in DMSO under an argon atmosphere via nanosecond time-resolved transient absorption spectroscopy

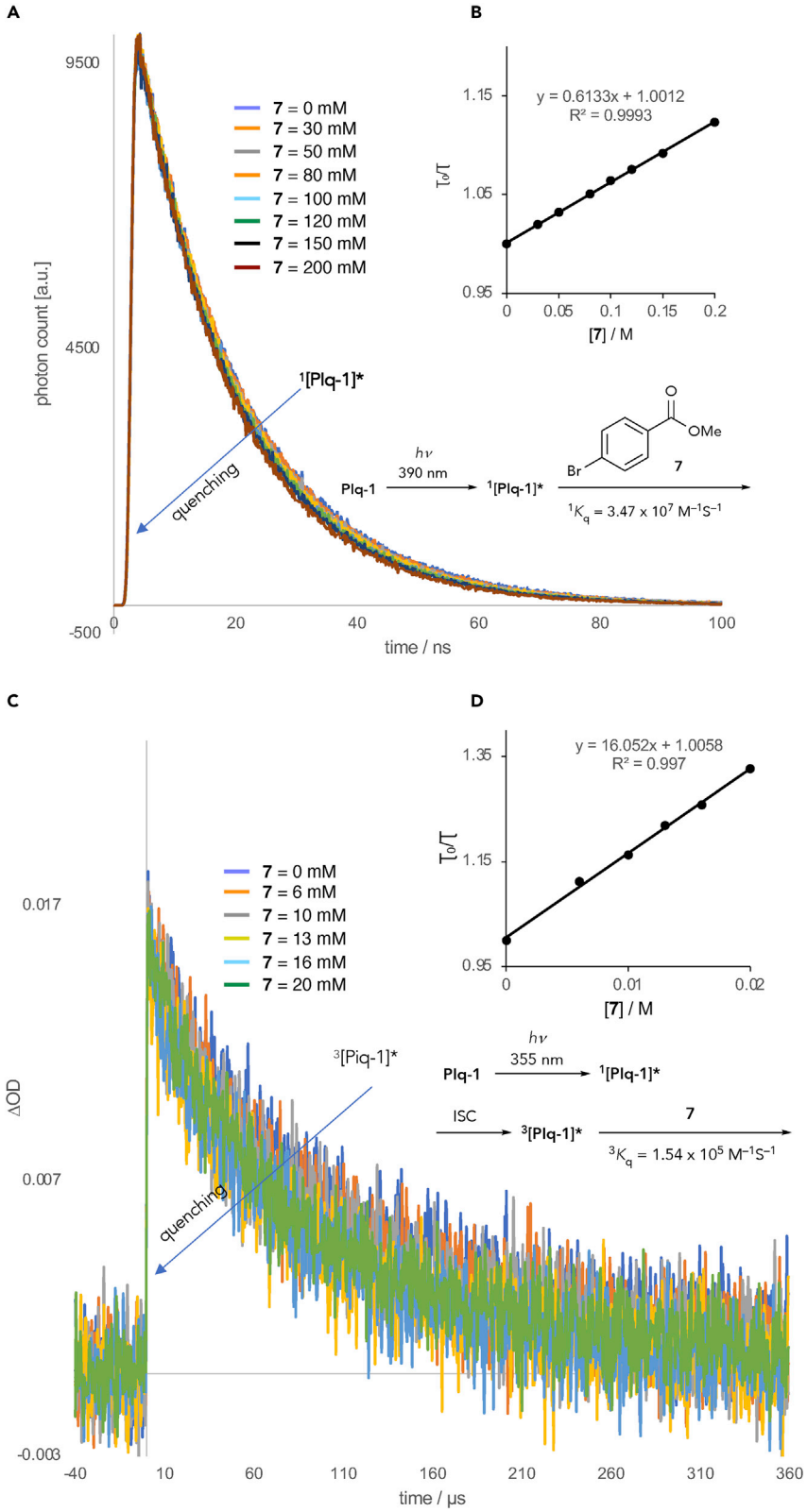

Figure 6. Quenching experiments of photoexcited states of Plq-1

(A) Monitoring of the fluorescence lifetime of **Plq-1** with methyl 4-bromobenzoate (**7**) in different concentrations by TCSPC.

Figure 6. *Continued*

(B) The Stern-Volmer plot to elucidate the dynamic quenching rate-constant (^1k_q = 3.47 × 10^7 M^{-1} s^{-1} at 293 K) of the S_1photoexcited state of **Plq-1** (see Table S8).

(C) Monitoring of the triplet (T_1) state lifetime of **Plq-1** with methyl 4-bromobenzoate (**7**) in different concentrations by the nanosecond-transient absorption spectroscopy using laser flash photolysis method at 355 nm (0.4 mJ/pulse, 4 ns pulse width). OD, optical density.

(D) The Stern-Volmer plot to elucidate the dynamic quenching rate-constant (^3k_q = 1.54 × 10^5 M^{-1} s^{-1} at 293 K) of the triplet photoexcited state of **Plq-1** (see Table S9).

by using the laser flash photolysis method at 355 nm (0.4 mJ/pulse, 4 ns pulse width) (Figures 6C and 6D). The decay rate constant of T_1, monitored by the T-T absorption at 360 nm, was measured in the presence of **7** in different concentrations (0–20 mM) at 293 K (Figure 6C). The lifetime ($^3\tau$ = 104.4 μs, ^3k_d = 9.6 × 10^3 s^{-1}) of the T_1 of **Plq-1** was also shortened in the presence of **7**: $^3\tau$ = 104.4 μs with [**7**] = 0 mM, $^3\tau$ = 93.4 μs with [**7**] = 6 mM, $^3\tau$ = 89.8 μs with [**7**] = 10 mM, $^3\tau$ = 85.6 μs with [**7**] = 13 mM, $^3\tau$ = 83.0 μs with [**7**] = 16 mM, and $^3\tau$ = 78.7 μs with [**7**] = 20 mM (Figure 6D). The quenching rate constant (^3k_q) was found to be 1.54 × 10^5 $M^{-1}s^{-1}$. Although the quenching rate constant of T_1 is 220 times smaller than that of S_1 (^1k_q = 3.47 × 10^7 $M^{-1}s^{-1}$), the quenching reaction mainly occurs in the T_1 state at relatively low concentrations of **7** such as less than 100 mM. At 100 mM of **7**, the quenching rate constant of S_1 by **7** was calculated to be 3.47 × 10^6 s^{-1}, which is smaller than the decay rate constant of S_1 (^1k_d = 5.65 × 10^7 s^{-1}). However, the quenching rate constant of T_1 by **7** was determined to be 1.54 × 10^4 s^{-1}, which is larger than the decay rate constant of T_1 (^3k_d = 9.6 × 10^3 s^{-1}). At the high concentration of **7** (>200 mM) in the cross-coupling reaction (entry 1 in Table 1), both the S_1 and T_1 states of **Plq-1** should play crucial roles in the SET reduction of **7**.

Ni-catalyzed amination and oxygenation of aryl halides

Synthetic utility of this Plq-based photoredox catalysis was further extended to nickel-catalyzed amination and oxygenation of aryl halides. Employment of photocatalysis

Table 3. Optimization of the reaction conditions for Ni-catalyzed amination

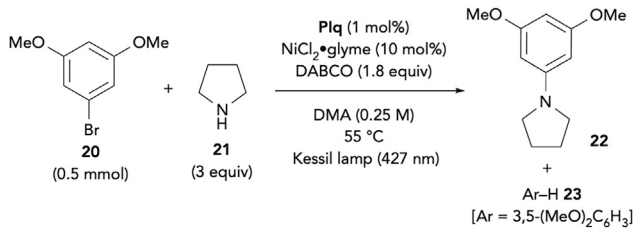

Entry	Plq	Conversion of 7 (%)[a]	Yield of 22 (%)[a]	Yield of 23 (%)[a]
1	**Plq-1**	>99	81 (79)[b]	8
2[c]	**Plq-1**	>86	74	6
3	no catalyst	2	<1	0
4[d]	**Plq-2**	>99	53	30
5	**Plq-3**	95	66	16
6	**Plq-4**	94	72	15
7	**Plq-5**	80	61	8
8	**Plq-6**	71	50	5

Reaction conditions: **20** (0.5 mmol), **21** (3 equiv), Plq (1 mol %), $NiCl_2$·glyme (10 mol %), DABCO (1.8 equiv), DMA (2 mL), 427 nm light (Kessil lamp), 55°C without fan cooling (see Figures S1 and S2).

[a]^{1}H NMR yields based on the internal standard.

[b]Isolated yield.

[c]The reaction was conducted with 0.2 mol % of **Plq-1**.

[d]Irradiation with 390 nm light.

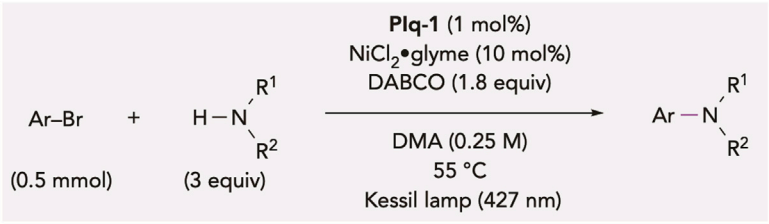

A Scope of aryl halides using pyrrolidine (21)

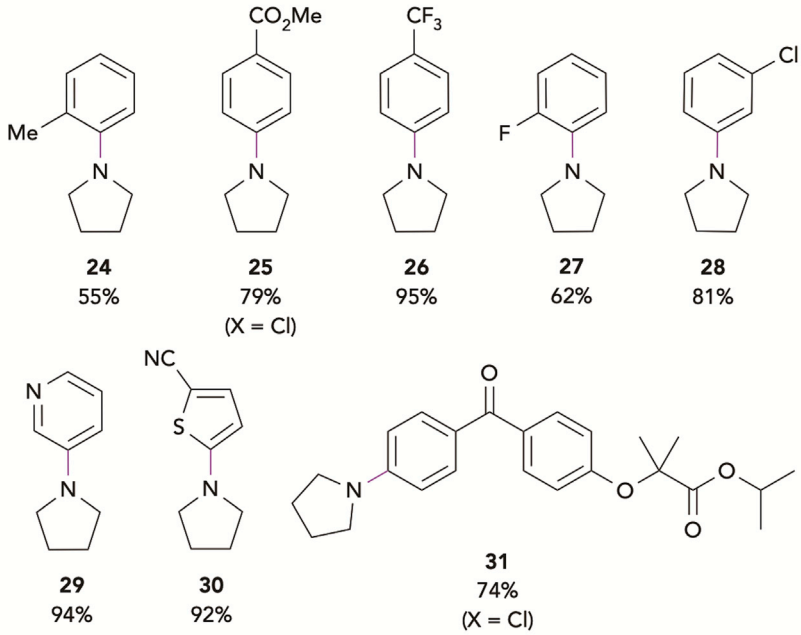

24 55%
25 79% (X = Cl)
26 95%
27 62%
28 81%
29 94%
30 92%
31 74% (X = Cl)

B Scope of amines using 3-bromopyridine

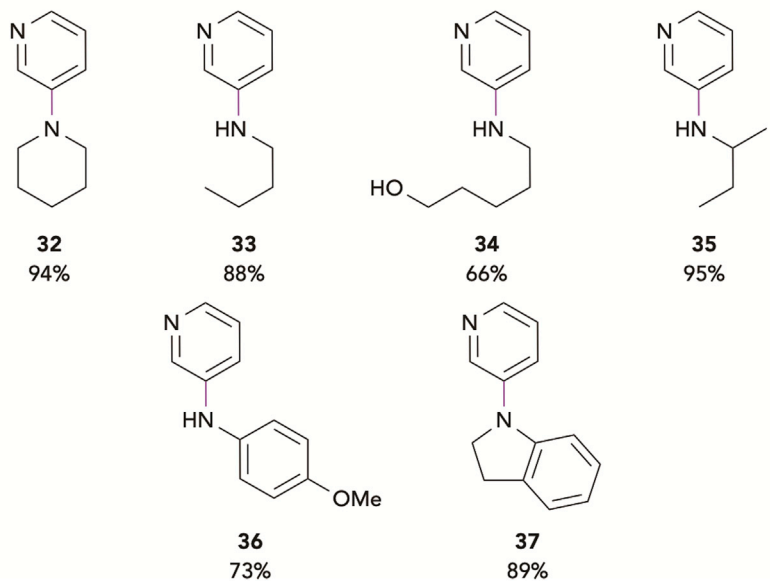

32 94%
33 88%
34 66%
35 95%
36 73%
37 89%

Figure 7. Substrate scope on Ni-catalyzed amination

Table 4. Optimization of the reaction conditions for Ni-catalyzed oxygenation

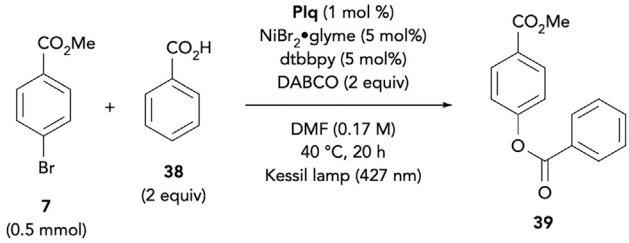

Entry	PIq	Conversion of 7 (%)[a]	Yield of 39 (%)[a]
1	**PIq-1**	>99	80 (76)[b]
2	no catalyst	9	4
3	**PIq-2**	>85 (390 nm)	43
4	**PIq-3**	>99	75
5	**PIq-4**	98	77
6	**PIq-5**	29	14
7	**PIq-6**	97	76

Reaction conditions: **7** (0.5 mmol), **38** (2 equiv), PIq (1 mol %), $NiBr_2$·glyme (5 mol %), dtbbpy (5 mol %), DABCO (2 equiv), DMF (3 mL), 427 nm light (Kessil lamp), 40°C without fan cooling (see Figures S1 and S2).
[a]^{1}H NMR yields based on the internal standard.
[b]Isolated yield.

in Ni-catalyzed cross-coupling processes can promote elemental organometallic processes such as oxidative addition and reductive elimination via the redox or EnT mechanism.[49] Thus, synergy between Ni-catalyzed cross-coupling and photocatalysis enables synthetically challenging bond-forging processes under milder reaction conditions. Typically, Ir polypyridyl complexes have been employed as the photocatalysts, while the use of organic chromophores in place of precious Ir complexes should be advantageous from the viewpoint of sustainability. First of all, we investigated Ni-catalyzed aryl amination, which was pioneered by MacMillan and Buchwald,[50] by using a substrate combination of 1-bromo-3,5-dimethoxybenzene (**20**) and pyrrolidine (**21**) (Tables 3 and S11). Treatment of a mixture of **20** with **21** (3 equiv) in the presence of $NiCl_2$·glyme (10 mol %), 1,4-diazabicyclo[2.2.2]octane (DABCO; 1.8 equiv), and **PIq-1** (1 mol %) in dimethylacetamide (DMA) under irradiation of 427 nm light at 55°C (no fan cooling) resulted in a full conversion of **20** within 24 h, providing 1-(3,5-dimethoxyphenyl)pyrrolidine (**22**) in 81% NMR yield (79% isolated yield) along with the formation of hydrodebromination product, 1,3-dimethoxybenzene (**23**), in 8% yield (entry 1). The catalyst loading of **PIq-1** could be reduced to 0.2 mol % without detrimental impact to the process (entry 2). Almost no conversion was observed in the absence of **PIq-1**, indicating that **PIq-1** functions as an indispensable redox mediator to promote the Ni-catalyzed C–N cross coupling (entry 3). **PIq-1** was found to be the best performing catalyst among a series of PIqs tested (entries 4–8).

We next examined the substituent compatibility of aryl halides for the Ni-catalyzed amination with pyrrolidine (**21**) by using **PIq-1** as the photocatalyst (Figure 7A). The protocol could engage sterically demanding 2-bromotoluene, providing **24** in 55% yield. As for electron-deficient aryl halides, the method could employ methyl 4-chlorobenzoate, 4-bromobenzotrifluoride, and 1-bromo-2-fluorobenzene to provide the corresponding aminated adducts **25**–**27** in good yields. The amination of 1-bromo-3-chlorobenzene was observed selectively at the bromide site to give **28** as a sole product while keeping the chloride site intact. The amination could be executed on heteroaryl halides based on pyridine (for **29**) and thiophene (for **30**).

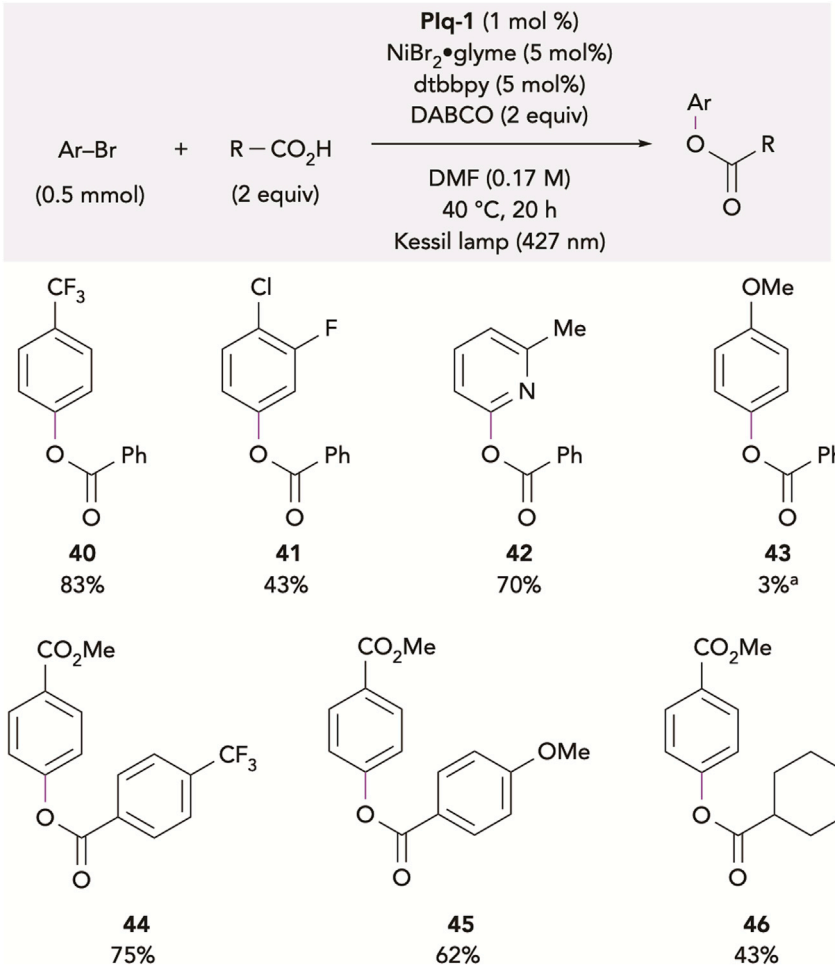

Figure 8. Substrate scope on Ni-catalyzed oxygenation

[a]^{1}H NMR yield of **43** based on the internal standard.

The protocol was amenable to the late-stage functionalization of a drug molecule, fenofibrate, to **31**. We then screened amines by using 3-bromopyridine as the coupling partner (Figure 7B). Amination with piperidine proceeded smoothly to afford **32**. Similarly, primary alkylamines could be engaged as the promising N nucleophiles (for **33**–**35**). When 5-amino-1-pentanol was employed, chemoselective pyridination was observed at the amine site (for **34**). The method was also found to be applicable to the amination with 4-methoxyaniline (for **36**) and indoline (for **37**).

MacMillan developed Ni-catalyzed C–O cross-coupling between aryl halides and carboxylic acids, where the Ir-based photocatalyst ($Ir(ppy)_3$) promotes reductive elimination of aryl esters aryl-Ni(II) carboxylate complexes via triplet sensitization or single-electron oxidation.[51,52] Given the high T_1 state energy and reasonable oxidizing ability of PIq, we surmised that the original Ir-based photocatalysts could be replaced with PIq for the Ni-catalyzed synthesis of aryl esters (Tables 4 and S12). As expected, the coupling reaction between methyl 4-bromobenzoate (**7**) and benzoic acid (**38**) was efficiently catalyzed by the $NiBr_2$·glyme-dtbbpy (5 mol %) system in the presence of **PIq-1** (1 mol %) and DABCO as a base under irradiation of 427 nm light, providing aryl ester **39** in 80% NMR yield (76% isolated yield) (entry 1). The control experiment without **PIq-1** resulted in poor conversion, proving its important role

Table 5. Optimization of the reaction conditions for decarboxylative cross-coupling

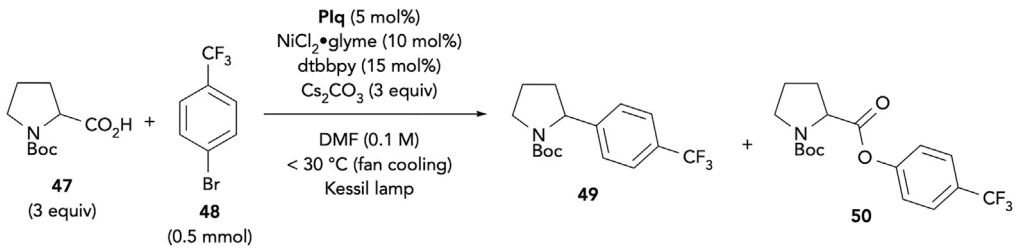

Entry	Plq	Wavelength (nm)	Conversion of 48 (%)[a]	Yield of 49 (%)[a]	Yield of 50 (%)[a]
1	**Plq-1**	427	58	14	30
2	no catalyst	427	15	0	0
3	no catalyst	390	35	0	20
4	**Plq-2**	390	>99	56	19
5	**Plq-6**	427	66	4	37

Reaction conditions: **47** (1.5 mmol, 3 equiv), **48** (0.5 mmol), Plq (5 mol %), $NiCl_2$·glyme (10 mol %), dtbbpy (15 mol %), Cs_2CO_3 (3 equiv), DMF (5 mL), 427 or 390 nm light (Kessil lamp), 30°C with fan cooling (see Figures S1 and S2).

[a]^{1}H NMR yields based on the internal standard.

to facilitate the catalysis (entry 2). Other Plqs (entries 3–7) also promoted the C–O cross coupling well except for **Plq-5** (entry 6), probably because of its lower triplet energy (2.43 eV, 56. 1 kcal mol^{-1}) and photoexcited reduction potential ($E^*_{red}{}^S$ = 0.61 V versus SCE).

This protocol could employ electron-deficient (hetero)aryl halides for the efficient construction of the corresponding aryl esters **40–42**, while the reaction with electron-rich 4-bromoanisole became sluggish (for **43**) (Figure 8). The coupling with 4-(trifluoromethyl)benzoic acid and 4-methoxybenzoic acid proceeded well (for **44** and **45**), and the method could be extended to the use of aliphatic carboxylic acid (for **46**).

Decarboxylative cross-coupling of α-amino carboxylic acids with aryl halides

We further aimed to expand the scope of the Plq photocatalysis to decarboxylative cross-coupling of α-amino acids and aryl halides. In the original precedent reported by MacMillan,[53,54] [Ir(dF(CF$_3$)ppy)$_2$(dtbbpy)]PF$_6$, whose photoexcited reduction potential E^*_{red} is 1.21 V versus SCE, was employed to promote single-electron oxidation of carboxylate salts for the formation of α-amino radicals, which are engaged in Ni-catalyzed cross-coupling cycle with aryl halides. By using *N*-Boc proline (**47**) (E_{ox} of the cesium carboxylate salt = 0.95 V versus SCE)[55] and 4-bromobenzotrifluoride (**48**) as the substrates, we investigated the probability to replace the Ir photocatalyst with **Plq-1**, **Plq-2**, or **Plq-6** (Tables 5 and S13).[56] The coupling reaction between **47** (3 equiv) and **48** catalyzed by the $NiCl_2$·glyme (10 mol %)-dtbbpy (15 mol %) in the presence of **Plq-1** (5 mol %) and Cs_2CO_3 as a base under irradiation with 427 nm of light gave the desired decarboxylative coupling product, 2-arylpyrrolidine **49**, in 14% yield along with a significant amount (30% yield) of aryl ester **50** via the C–O cross-coupling as a co-product (entry 1). We confirmed that no background coupling was observed in the absence of **Plq-1** under irradiation with 427 nm light (entry 2). However, under irradiation with 390 nm light, we observed the slow formation of aryl ester **50** in 20% yield, indicating that direct photoexcitation of aryl esters aryl-Ni(II) carboxylate complexes facilitates the C–O reductive elimination to some extent (entry 3). In turn, the reaction of **Plq-2**, which showed higher photoexcited reduction potential ($E^*_{red}{}^S$ = 1.09 V), under irradiation

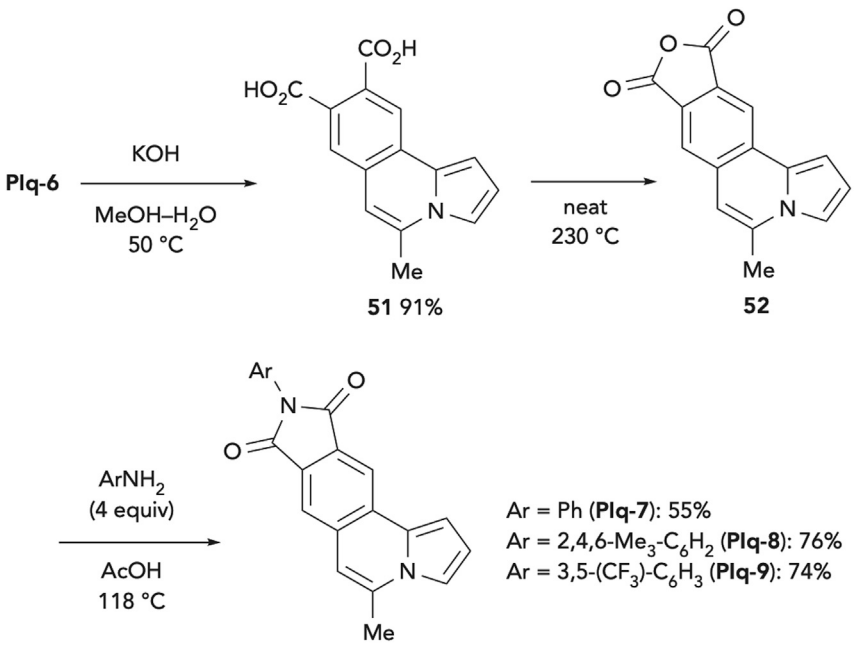

Figure 9. Synthesis of PIq-7 to PIq-9 with an *N*-arylphthalimide moiety

with 390 nm light, selectively promoted the decarboxylative cross-coupling (56% yield of **49**) over the C–O coupling (19% yield of **50**) (entry 4), whereas **PIq-6**, possessing two methoxy carbonyl groups, gave aryl ester **50** as the major product (entry 5).

To further improve the process efficiency for the decarboxylative cross-coupling by mitigating the undesired C–O cross-coupling, we aimed to modify the PIq scaffold. For this purpose, we became interested in the introduction of an *N*-arylphthalimide moiety, which has high electron affinity and good charge carrier mobility, as well as high thermal and redox stability,[57,58] and thus has been utilized as the important function for the generation of stabilized radical anion species.[39,59,60] First of all, **PIq-6** was converted into anhydride **52** via basic hydrolysis of the diester moiety of **PIq-6** to dicarboxylic acid **51** and its subsequent dehydration (Figure 9). Treatment of anhydride **52** with arylamines in acetic acid then led to the formation of **PIq-7** to **PIq-9** with an *N*-arylimide moiety.

A set of photophysical and electrochemical analyses of **PIq-7** to **PIq-9** revealed that they showed extremely weak fluorescence emissivity with lower quantum yields and shorter fluorescence lifetimes (Table 6). Therefore, we assumed that **PIq-7** to **PIq-9** could perform photoredox processes in the T_1 states. It turned out that they exhibit enhanced photoexcited reduction potential E^*_{red}, whereas their reducing ability in their photoexcited state becomes weakened and their excitation energies in their T_1 states are relatively lower ($E_{0,0}{}^T$ = 2.35–2.38 eV). Especially, **PIq-9** showed higher oxidizing ability ($E^*_{red}{}^T$ = 1.06 V versus SCE) in its T_1 state ($E_{0,0}{}^T$ = 2.36 eV, 54.4 kcal mol^{-1}) with a longer lifetime (141 μs) (entry 3).

We were pleased to observe the improved selectivity for the decarboxylative cross-coupling of **47** and **48** with **PIq-7** to **PIq-9** (Table 7), and as expected, **PIq-9** exhibited the best performance, affording **49** in 76% NMR yield (71% isolated yield) while minimizing the C–O coupling product **50** in 6% yield (entry 3).

Table 6. Photophysical and electrochemical characterization of PIq-7 to PIq-9

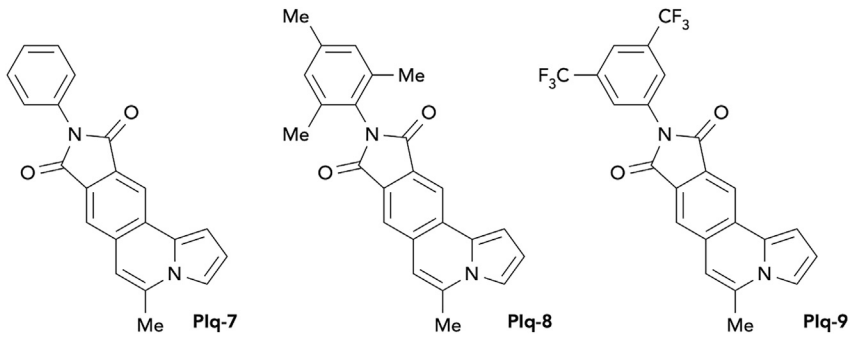

Entry	PIq	MW	$\lambda_{abs/em\ max}$ (nm)[a]	Φ (fl)[b]	τ (S_1) (ns)[c]	τ (T_1) (μs)[d]	$E_{0,0}$ (eV)[e]	E_{ox} (V)[f]	E_{red} (V)[f]	E^*_{ox} (V)[g]	E^*_{red} (V)[h]
1	**PIq-7**	326.36	366/602	0.024	2.24	25	2.56 (S_1), 2.38 (T_1)	1.13	−1.40	−1.43 (S_1), −1.25 (T_1)	1.16 (S_1), 0.98 (T_1)
2	**PIq-8**	368.44	368/592	0.032	2.99	37	2.54 (S_1), 2.35 (T_1)	1.13	−1.42	−1.41 (S_1), −1.22 (T_1)	1.12 (S_1), 0.93 (T_1)
3	**PIq-9**	462.35	370/592	0.010	τ_1: 1.04 (95%); τ_2: 5.77 (5%)	141	2.60 (S_1), 2.36 (T_1)	1.14	−1.30	−1.46 (S_1), −1.22 (T_1)	1.30 (S_1), 1.06 (T_1)

[a]The lowest energy absorption maxima and the highest energy fluorescence emission maxima measured in DMSO (see Figures S33, S36, and S39).
[b]Fluorescence quantum yields.
[c]Lifetime of S_1 states determined by TCSPC (see Figures S34, S37, and S40).
[d]Lifetime of T_1 states measured by transient absorption spectroscopy (see Figures S35, S38, and S41).
[e]Excitation energies ($E_{0,0}$) for the S_1 and T_1 states. $E_{0,0}$ for S_1 were taken from the intersection of the absorption and fluorescence emission bands. $E_{0,0}$ for T_1 were estimated from the onset of the phosphorescence emission spectra.
[f]The electrochemical potentials (V versus SCE) measured by CV (see Figures S53–S55).
[g]Photoexcited oxidation potentials in S_1 and T_1 states calculated using $E_{0,0}$ and E_{ox}.
[h]Photoexcited reduction potentials in S_1 and T_1 states calculated using $E_{0,0}$ and E_{red}.

With **PIq-9** as the photocatalyst, we then examined the scope and limitation of the decarboxylative cross-coupling reactions (Figure 10). With respect to aryl bromides (Figure 10A), the protocol could install electron-deficient aryl groups (for **53** and **54**), while the reaction with electron-rich 4-bromoanisole resulted in moderate efficiency (for **55**). The cross-coupling with 1-bromo-4-chlorobenzene was observed selectively at the bromide site (for **56**). The method is amenable to introduce a 3-pyridyl moiety onto the pyrrolidine scaffold (for **57**). As for carboxylic acids (Figure 10B), the method

Table 7. Screening of PIq-7–9 for decarboxylative cross-coupling

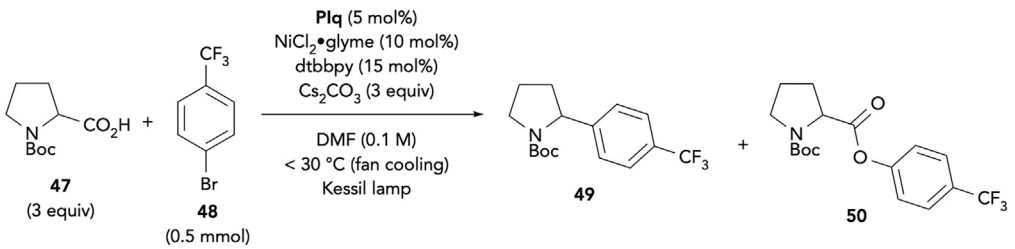

Entry	PIq	Conversion of 48 (%)[a]	Yield of 49 (%)[a]	Yield of 50 (%)[a]
1	**PIq-7**	>99	51	12
2	**PIq-8**	>99	71	19
3	**PIq-9**	>99	76 (71)[b]	6

Reaction conditions: **47** (1.5 mmol, 3 equiv), **48** (0.5 mmol), PIq (5 mol %), $NiCl_2$·glyme (10 mol %), dtbbpy (15 mol %), Cs_2CO_3 (3 equiv), DMF (5 mL), 390 nm light (Kessil lamp), 30°C with fan cooling (see Figures S1 and S2).
[a]^{1}H NMR yields based on the internal standard.
[b]Isolated yield.

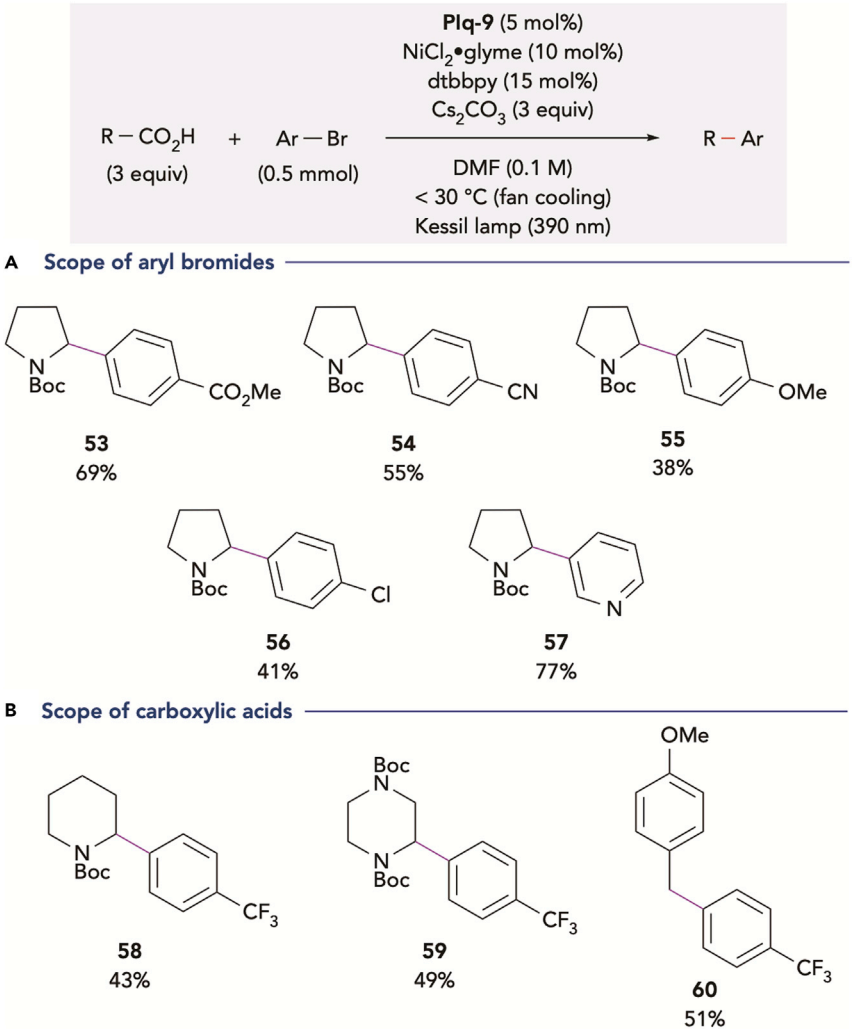

Figure 10. Substrate scope on decarboxylative cross-coupling

could employ those based on piperidine and pyrazine scaffolds (for **58** and **59**). Moreover, the decarboxylative cross-coupling of 4-methoxyphenylacetic acid and 4-bromobenzotrifluoride afforded unsymmetrical diarylmethane **60** in 51% yield.

Molecular transformations via triplet-triplet sensitization

Given that **PIq-1** possesses reasonably high T_1 state energy of nearly 60 kcal/mol, we next tested engagement of **PIq-1** as the photocatalyst to drive molecular transformations triggered by triplet-triplet sensitization of the substrates (Figure 11). We first examined intermolecular [2 + 2]-cycloaddition between chalcone (**61**) and 1,1-diphenylethylene (**62**), which was previously catalyzed by $Ir(ppy)_3$ as the photosensitizing catalyst.[61] We found that **PIq-1** could play as a substitute for $Ir(ppy)_3$ to form cyclobutane **63** in 69% yield (Figure 11A). Similarly, **PIq-1** could promote efficiently intramolecular [2 + 2]-cycloaddition reactions of *N*-alkenyl cinnamamides **64** and **65** under irradiation with 427 nm light, affording bicyclic pyrrolidone **66** and piperidone **67**, respectively, in excellent yields (Figure 11B).[62] **PIq-1** could also be used as a radical chain initiator for the degenerative transfer of xanthate **68** to alkene **69**, which was previously promoted by $[Ir(dF(CF_3)ppy)_2(dtbbpy)]PF_6$ as the photosensitizer (Figure 11C).[63] Schindler recently discovered that *fac*-$Ir(dFppy)_3$, whose T_1 state energy

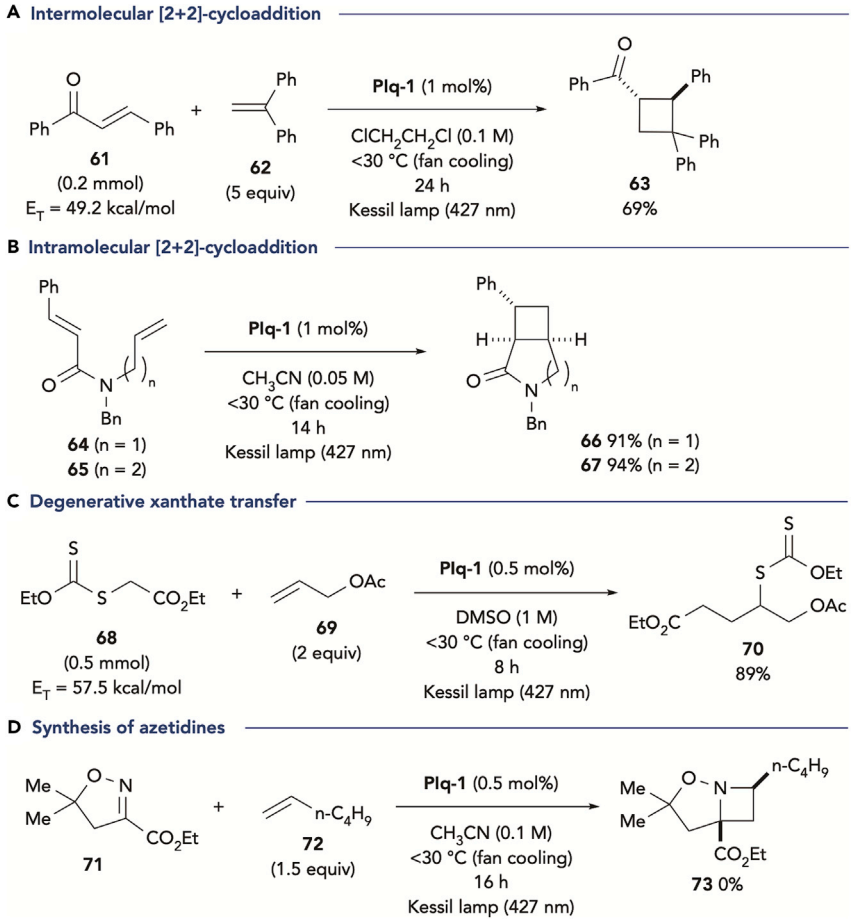

Figure 11. Molecular transformations via triplet sensitization by Plq-1

is 60.1 kcal mol^{-1}, can be employed as an efficient photosensitizer to promote aza Paternò-Büchi [2 + 2]-cycloaddition between 2-isoxazoline-3-carboxylates and alkenes, enabling a facile construction of an array of complex azetidines.[64,65] We also tested utilization of **Plq-1** as an organic substitute for the Ir photocatalyst to catalyze [2 + 2]-photocycloaddition between isoxazoline-3-carboxylate **71** and 1-hexene (**72**) (Figure 11D). However, it turned out that **Plq-1** is incapable of catalyzing the process. This is probably due to the unproductive SET processes between **71** (E_{red} = −2.01 V versus SCE) and photoexcited **Plq-1** ($E^*_{ox}{}^{S}$ = −2.06 V versus SCE), which hampers the desired EnT process. To prevent this undesired redox process, it is necessary to lower the reducing ability of Plq while maintaining reasonably high triplet energy.

During the course of our study in photoredox processes of **Plq-1** with cyanoarenes,[66] we found that the treatment of **Plq-1** with 4-cyanopyridine (**74**) in the presence of potassium cyanide (KCN; 3 equiv) under irradiation with 427 nm light affords **Plq-10** having a cyano group on the pyrrole moiety (Figure 12). The process could be initiated by the photoinduced SET between **Plq-1** and **74** (E_{red} = −1.84 V versus SCE)[67] to generate a cation radical of **Plq-1**. Interception of the cation radical by a cyanide ion and subsequent oxidative re-aromatization could liberate **Plq-10**.

As a result of an additional cyano group, the photoexcited oxidation potential ($E^*_{ox}{}^{S}$) of **Plq-10** became less negative (−1.74 V versus SCE), although the T_1 state

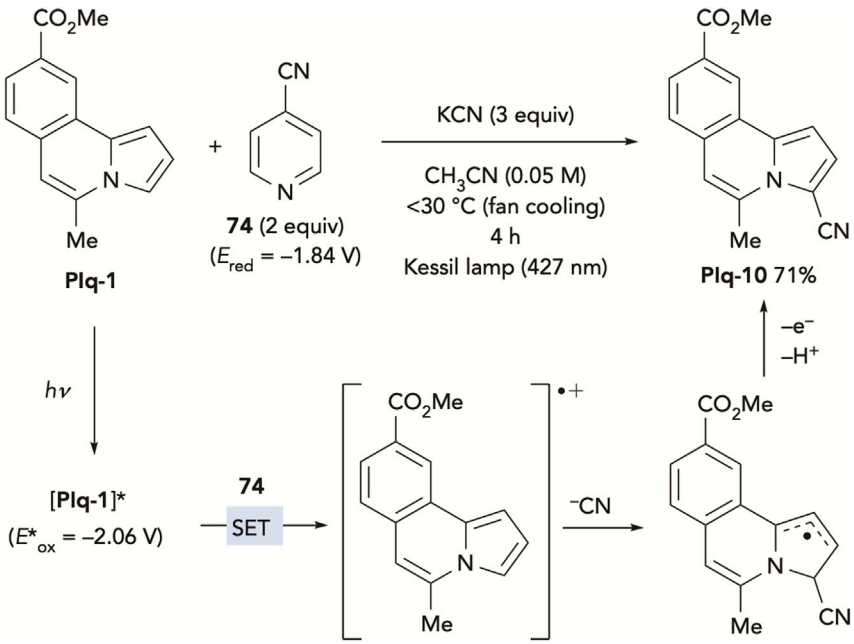

Figure 12. Photoinduced cyanation of Plq-1

energy remained high (2.66 eV, 61.3 kcal mol^{-1}) (Table 8).[68] We were pleased to observe that **Plq-10** is capable of catalyzing aza Paternò-Büchi [2 + 2]-cycloaddition of isoxazoline-3-carboxylate **71** with a series of alkenes under irradiation with 390 nm light (Figure 13 and Table S14). The protocol could engage not only mono- and disubstituted terminal alkenes (for **73**, **75** and **76**) but also internal alkenes such as cyclohexene (for **77**) and 1,1,2,2-tetramethylethylene (for **78**), providing the corresponding azetidines in good to moderate yields. We also found that the method could employ terminal alkyne for the construction of 2-azetine **79** in 41% yield.[69]

Table 8. Photophysical and electrochemical comparison between Plq-1 and Plq-10

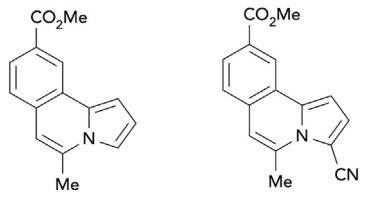

Entry	Plq	$\lambda_{abs/em\ max}$ (nm)[a]	τ (T_1) (μs)[b]	$E_{0,0}$ (eV)[c]	$E^*_{ox}{}^S$ (V)[d]	$E^*_{red}{}^S$ (V)[e]
1	**Plq-1**	380/490	104	2.90 (S_1), 2.58 (T_1)	−2.06	0.86
2	**Plq-10**	363/445	25	3.11 (S_1), 2.66 (T_1)	−1.74	1.24

[a]The lowest energy absorption maxima and the highest energy fluorescence emission maxima measured in DMSO (see Figures S42).
[b]Lifetime of T_1 states measured by transient absorption spectroscopy (see Figures S43 and S44).
[c]Excitation energies ($E_{0,0}$) for the S_1 and T_1 states. $E_{0,0}$ for S_1 were taken from the intersection of the absorption and fluorescence emission bands. $E_{0,0}$ for T_1 were estimated from the onset of the phosphorescence emission spectra.
[d]Photoexcited oxidation potentials in S_1 states calculated with $E_{0,0}$ and E_{ox} (see Figure S56).
[e]Photoexcited reduction potentials in S_1 states calculated with $E_{0,0}$ and E_{red} (see Figure S56).

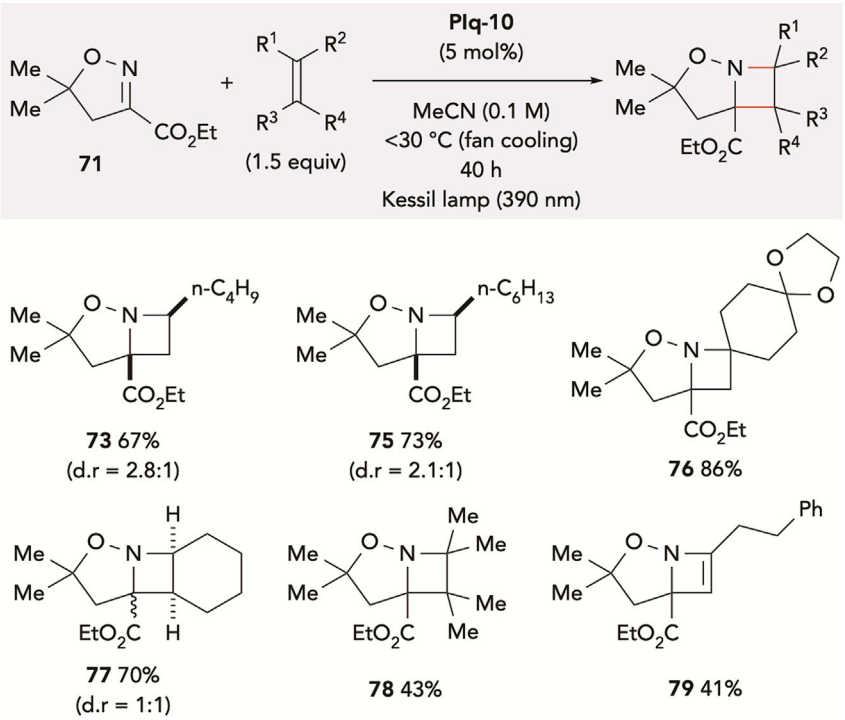

Figure 13. Photoinduced aza Paternò-Büchi reaction catalyzed by PIq-10

Conclusion

We have shown that planar and compact PIqs bearing EWGs can perform various photocatalytic molecular formations via SET and EnT processes under irradiation with visible light. The photophysical and electrochemical characters can be tuned through the modification of EWGs and changing their positions on the PIq scaffold to promote the desired photochemical processes, including redox-neutral (hetero) biaryl cross-coupling between aryl halides and (hetero)arenes, nickel-catalyzed aryl amination and oxygenation of aryl halides, and nickel-catalyzed decarboxylative cross-coupling between α-amino acids and aryl halides, as well as a set of the transformations driven by triplet-triplet sensitization. It should be noted that PIqs could be prepared by operationally simple and transition-metal-free protocols. We view the present design principle of PIqs as a useful tool for tailoring organo-based photocatalysts of demand in various synthetic endeavors.

EXPERIMENTAL PROCEDURES

Resource availability

Lead contact

Further information and requests for resources should be directed to and will be fulfilled by the lead contact, Shunsuke Chiba (shunsuke@ntu.edu.sg).

Materials availability

All other data supporting the findings of this study are available within the article and the supplemental information or from the lead contact upon reasonable request.

Data and code availability

Data relating to the materials and methods, experimental procedures, X-ray crystallographic data (Tables S1–S6 and Figures S3–S8), and NMR spectra

(Figures S65–S253) are available in the supplemental information. All other data are available from the authors upon reasonable request.

SUPPLEMENTAL INFORMATION

Supplemental information can be found online at https://doi.org/10.1016/j.checat.2022.08.013.

ACKNOWLEDGMENTS

Financial support was provided by Nanyang Technological University (NTU) and the Singapore Ministry of Education (Academic Research Fund Tier 2: MOE2017-T2-1-064) (to S.C.), as well as JSPS KAKENHI grants (JP21H01921 and JP20K21197) and the Uehara Memorial Foundation (to M.A.). We acknowledge Dr. Yongxin Li (Division of Chemistry and Biological Chemistry, NTU) for assistance in X-ray crystallographic analysis. We thank Jean-Philippe Krieger (Syngenta) and Farhan Bou Hamdan (Syngenta) for helpful discussion.

AUTHOR CONTRIBUTIONS

Conceptualization and methodology, Y.L., M.A., and S.C.; investigation, Y.L., H.L., E.Y.K.T., E.B.S., and Y.C.; writing – original draft, Y.L., M.A., and S.C.; writing – review & editing, S.C.; funding acquisition, resources, and supervision, M.A. and S.C.

DECLARATION OF INTERESTS

The authors declare no competing interests.

Received: July 18, 2022
Revised: August 11, 2022
Accepted: August 23, 2022
Published: September 14, 2022

REFERENCES

1. Bell, J.D., and Murphy, J.A. (2021). Recent advances in visible light-activated radical coupling reactions triggered by (i) ruthenium, (ii) iridium and (iii) organic photoredox agents. Chem. Soc. Rev. *50*, 9540–9685.
2. Crisenza, G.E.M., and Melchiorre, P. (2020). Chemistry grows green with photoredox catalysis. Nat. Commun. *11*, 803.
3. McAtee, R.C., McClain, E.J., and Stephenson, C.R. (2019). Illuminating photoredox catalysis. Trends Chem. *1*, 111–125.
4. Marzo, L., Pagire, S.K., Reiser, O., and König, B. (2018). Visible-light photocatalysis: Does it make a difference in organic synthesis? Angew. Chem. Int. Ed. *57*, 10034–10072.
5. Ravelli, D., Protti, S., and Fagnoni, M. (2016). Carbon-carbon bond forming reactions via photogenerated intermediates. Chem. Rev. *116*, 9850–9913.
6. Shaw, M.H., Twilton, J., and MacMillan, D.W.C. (2016). Photoredox catalysis in organic chemistry. J. Org. Chem. *81*, 6898–6926.
7. Zhang, N., Samanta, S.R., Rosen, B.M., and Percec, V. (2014). Single electron transfer in radical ion and radical-mediated organic, materials and polymer synthesis. Chem. Rev. *114*, 5848–5958.
8. Teets, T.S., Wu, Y., and Kim, D. (2022). Photophysical properties and redox potentials of photosensitizers for organic photoredox transformations. Synlett *33*, 1154–1179.
9. Cao, H., Tang, X., Tang, H., Yuan, Y., and Wu, J. (2021). Photoinduced intermolecular hydrogen atom transfer reactions in organic synthesis. Chem Catal. *1*, 523–598.
10. Capaldo, L., Ravelli, D., and Fagnoni, M. (2022). Direct photocatalyzed hydrogen atom transfer (HAT) for aliphatic C–H bonds elaboration. Chem. Rev. *122*, 1875–1924.
11. Holmberg-Douglas, N., and Nicewicz, D.A. (2022). Photoredox-catalyzed C–H functionalization reactions. Chem. Rev. *122*, 1925–2016.
12. Strieth-Kalthoff, F., and Glorius, F. (2020). Triplet energy transfer photocatalysis: Unlocking the next level. Chem *6*, 1888–1903.
13. Strieth-Kalthoff, F., James, M.J., Teders, M., Pitzer, L., and Glorius, F. (2018). Energy transfer catalysis mediated by visible light: Principles, applications, directions. Chem. Soc. Rev. *47*, 7190–7202.
14. Romero, N.A., and Nicewicz, D.A. (2016). Organic photoredox catalysis. Chem. Rev. *116*, 10075–10166.
15. Vega-Peñaloza, A., Mateos, J., Companyó, X., Escudero-Casao, M., and Dell'Amico, L. (2021). A rational approach to organo-photocatalysis: Novel designs and structure-property relationships. Angew. Chem. Int. Ed. *60*, 1082–1097.
16. Tlili, A., and Lakhdar, S. (2021). Acridinium salts and cyanoarenes as powerful photocatalysts: Opportunities in organic synthesis. Angew. Chem. Int. Ed. *60*, 19526–19549.
17. Turro, N.J., Ramamurthy, V., and Scaiano, J.C. (2010). Modern Molecular Photochemistry of Organic Molecules (Sausalito, California: University Science Books).
18. Discekici, E.H., Treat, N.J., Poelma, S.O., Mattson, K.M., Hudson, Z.M., Luo, Y., Hawker, C.J., and Read de Alaniz, J. (2015). Highly reducing metal-free photoredox catalyst: Design and application in radical dehalogenations. Chem. Commun. *51*, 11705–11708.
19. Sartor, S.M., Chrisman, C.H., Pearson, R.M., Miyake, G.M., and Damrauer, N.H. (2020). Designing high-triplet-yield phenothiazine donor-acceptor complexes for photoredox catalysis. J. Phys. Chem. A *124*, 817–823.
20. Romero, N.A., and Nicewicz, D.A. (2014). Mechanistic insight into the photoredox

catalysis of anti-Markovnikov alkene hydrofunctionalization reactions. J. Am. Chem. Soc. *136*, 17024–17035.

21. Uoyama, H., Goushi, K., Shizu, K., Nomura, H., and Adachi, C. (2012). Highly efficient organic light-emitting diodes from delayed fluorescence. Nature *492*, 234–238.

22. Yang, Z., Mao, Z., Xie, Z., Zhang, Y., Liu, S., Zhao, J., Xu, J., Chi, Z., and Aldred, M.P. (2017). Recent advances in organic thermally activated delayed fluorescence materials. Chem. Soc. Rev. *46*, 915–1016.

23. Bryden, M.A., and Zysman-Colman, E. (2021). Organic thermally activated delayed fluorescence (TADF) compounds used in photocatalysis. Chem. Soc. Rev. *50*, 7587–7680.

24. Shang, T.-Y., Lu, L.-H., Cao, Z., Liu, Y., He, W.-M., and Yu, B. (2019). Recent advances of 1, 2, 3, 5-tetrakis(carbazole-9-yl)-4, 6-dicyanobenzene (4CzIPN) in photocatalytic transformations. Chem. Commun. *55*, 5408–5419.

25. Speckmeier, E., Fischer, T.G., and Zeitler, K. (2018). Toolbox approach to construct broadly applicable metal-free catalysts for photoredox chemistry: Deliberate tuning of redox potentials and importance of halogens in donor-acceptor cyanoarenes. J. Am. Chem. Soc. *140*, 15353–15365.

26. Sartor, S.M., McCarthy, B.G., Pearson, R.M., Miyake, G.M., and Damrauer, N.H. (2018). Exploiting charge-transfer states for maximizing intersystem crossing yields in organic photoredox catalysts. J. Am. Chem. Soc. *140*, 4778–4781.

27. McCarthy, B.G., Pearson, R.M., Lim, C.-H., Sartor, S.M., Damrauer, N.H., and Miyake, G.M. (2018). Structure–property relationships for tailoring phenoxazines as reducing catalysts. J. Am. Chem. Soc. *140*, 5088–5101.

28. Du, Y., Pearson, R.M., Lim, C.-H., Sartor, S.M., Ryan, M.D., Yang, H., Damrauer, N.H., and Miyake, G.M. (2017). Strongly reducing, visible-light organic photoredox catalysts as sustainable alternatives to precious metals. Chemistry *23*, 10962–10968.

29. Pearson, R.M., Lim, C.-H., McCarthy, B.G., Musgrave, C.B., and Miyake, G.M. (2016). Organocatalyzed atom transfer radical polymerization using N-aryl phenoxazines as photoredox catalysts. J. Am. Chem. Soc. *138*, 11399–11407.

30. Corbin, D.A., and Miyake, G.M. (2022). Photoinduced organocatalyzed atom transfer radical polymerization (O-ATRP): Precision polymer synthesis using organic photoredox catalysis. Chem. Rev. *122*, 1830–1874.

31. Endo, A., Sato, K., Yoshimura, K., Kai, T., Kawada, A., Miyazaki, H., and Adachi, C. (2011). Efficient up-conversion of triplet excitons into a singlet state and its application for organic light emitting diodes. Appl. Phys. Lett. *98*, 083302.

32. Wang, L., Byun, J., Li, R., Huang, W., and Zhang, K.A.I. (2018). Molecular design of donor-acceptor-type organic photocatalysts for metal-free aromatic C-C bond formations under visible light. Adv. Synth. Catal. *360*, 4312–4318.

33. Wakamiya, A., Mori, K., and Yamaguchi, S. (2007). 3-Boryl-2,2′-bithiophene as a versatile core skeleton for full-color highly emissive organic solids. Angew. Chem. Int. Ed. *46*, 4273–4276.

34. Liu, Y., Li, H., and Chiba, S. (2021). Photoinduced cross-coupling of aryl iodides with alkenes. Org. Lett. *23*, 427–432.

35. Hayashi, H., Wang, B., Wu, X., Teo, S.J., Kaga, A., Watanabe, K., Takita, R., Yeow, E.K.L., and Chiba, S. (2020). Biaryl cross-coupling enabled by photo-induced electron transfer. Adv. Synth. Catal. *362*, 2223–2231.

36. Reichardt, C. (2003). In Solvents and Solvent effects in organic chemistry, 3rd ed. (Wiley-VCH), Chapter 6.

37. Kvasovs, N., and Gevorgyan, V. (2021). Contemporary methods for generation of aryl radicals. Chem. Soc. Rev. *50*, 2244–2259.

38. Ghosh, I., Marzo, L., Das, A., Shaikh, R., and König, B. (2016). Visible light mediated photoredox catalytic arylation reactions. Acc. Chem. Res. *49*, 1566–1577.

39. Ghosh, I., Ghosh, T., Bardagi, J.I., and König, B. (2014). Reduction of aryl halides by consecutive visible light-induced electron transfer processes. Science *346*, 725–728.

40. Ghosh, I., and König, B. (2016). Chromoselective photocatalysis: controlled bond activation through light-color regulation of redox potentials. Angew. Chem. Int. Ed. *55*, 7676–7679.

41. Neumeier, M., Sampedro, D., Májek, M., de la Peña O'Shea, V.A., Jacobi von Wangelin, A., and Pérez-Ruiz, R. (2018). Dichromatic photocatalytic substitutions of aryl halides with a small organic dye. Chemistry *24*, 105–108.

42. Li, Y., Ye, Z., Lin, Y.-M., Liu, Y., Zhang, Y., and Gong, L. (2021). Organophotocatalytic selective deuterodehalogenation of aryl or alkyl chlorides. Nat. Commun. *12*, 2894.

43. Li, H., Tang, X., Pang, J.H., Wu, X., Yeow, E.K.L., Wu, J., and Chiba, S. (2021). Polysulfide anions as visible light photoredox catalysts for aryl cross-coupling. J. Am. Chem. Soc. *143*, 481–487.

44. It should be noted that photoexcitation of **PIq-2** requires irradiation with UVA (390 nm) light. The heterobiaryl cross-coupling reaction by **PIq-2** (1 mol %) under irradiation of 390 nm light provided 2 in 85% yield (full conversion, 24 h), whereas the reaction in the absence of **PIq-2** also gave 2 in 62% yield (90% conversion, 24 h).

45. Meng, G., Li, P., Chen, K., and Wang, L. (2017). Recent advances in transition-metal-free aryl C–B bond formation. Synthesis *49*, 4719–4730.

46. Jin, S., Dang, H.T., Haug, G.C., He, R., Nguyen, V.D., Nguyen, V.T., Arman, H.D., Schanze, K.S., and Larionov, O.V. (2020). Visible light-induced borylation of C-O, C-N, and C-X bonds. J. Am. Chem. Soc. *142*, 1603–1613.

47. Jiang, M., Yang, H., and Fu, H. (2016). Visible-light photoredox borylation of aryl halides and subsequent aerobic oxidative hydroxylation. Org. Lett. *18*, 5248–5251.

48. Shaikh, R.S., Düsel, S.J.S., and König, B. (2016). Visible-light photo-arbuzov reaction of aryl bromides and trialkyl phosphites yielding aryl phosphonates. ACS Catal. *6*, 8410–8414.

49. Twilton, J., Le, C., Zhang, P., Shaw, M.H., Evans, R.W., and MacMillan, D.W.C. (2017). The merger of transition metal and photocatalysis. Nat. Rev. Chem *1*, 0052.

50. Corcoran, E.B., Pirnot, M.T., Lin, S., Dreher, S.D., DiRocco, D.A., Davies, I.W., Buchwald, S.L., and MacMillan, D.W.C. (2016). Aryl amination using ligand-free Ni(II) salts and photoredox catalysis. Science *353*, 279–283.

51. Welin, E.R., Le, C., Arias-Rotondo, D.M., McCusker, J.K., and MacMillan, D.W.C. (2017). Photosensitized, energy transfer-mediated organometallic catalysis through electronically excited nickel(II). Science *355*, 380–385.

52. Tian, L., Till, N.A., Kudisch, B., MacMillan, D.W.C., and Scholes, G.D. (2020). Transient absorption spectroscopy offers mechanistic insight for an iridium/nickel-catalyzed C–O coupling. J. Am. Chem. Soc. *142*, 4555–4559.

53. Zuo, Z., Ahneman, D.T., Chu, L., Terrett, J.A., Doyle, A.G., and MacMillan, D.W.C. (2014). Merging photoredox with nickel catalysis: Coupling of a-carboxyl sp^3-carbons with aryl halides. Science *345*, 437–440.

54. Zuo, Z., Cong, H., Li, W., Choi, J., Fu, G.C., and MacMillan, D.W.C. (2016). Enantioselective decarboxylative arylation of α-amino acids via the merger of photoredox and nickel catalysis. J. Am. Chem. Soc. *138*, 1832–1835.

55. Zuo, Z., and MacMillan, D.W.C. (2014). Decarboxylative arylation of α-amino acids via photoredox catalysis: A one-step conversion of biomass to drug pharmacophore. J. Am. Chem. Soc. *136*, 5257–5260.

56. Luo, J., and Zhang, J. (2016). Donor–acceptor fluorophores for visible-light-promoted organic synthesis: Photoredox/Ni dual catalytic $C(sp^3)$–$C(sp^2)$ cross-coupling. ACS Catal. *6*, 873–877.

57. Demeter, A., Bérces, T., Biczók, L., Wintgens, V., Valat, P., and Kossanyi, J. (1996). Comprehensive model of the photophysics of N-phenylnaphthalimides: The role of solvent and rotational relaxation. J. Phys. Chem. *100*, 2001–2011.

58. Andric, G., Boas, J.F., Bond, A.M., Fallon, G.D., Ghiggino, K.P., Hogan, C.F., Hutchison, J.A., Lee, M.A.-P., Langford, S.J., Pilbrow, J.R., et al. (2004). Spectroscopy of naphthalene diimides and their anion radicals. Aust. J. Chem. *57*, 1011–1019.

59. Cowper, N.G.W., Chernowsky, C.P., Williams, O.P., and Wickens, Z.K. (2020). Potent reductants via electron-primed photoredox catalysis: unlocking aryl chlorides for radical coupling. J. Am. Chem. Soc. *142*, 2093–2099.

60. Tian, X., Karl, T.A., Reiter, S., Yakubov, S., de Vivie-Riedle, R., König, B., and Barham, J.P. (2021). Electro-mediated photoredox catalysis for selective $C(sp^3)$-O cleavages of phosphinated alcohols to carbanions. Angew. Chem. Int. Ed. *60*, 20817–20825.

61. Lei, T., Zhou, C., Huang, M.-Y., Zhao, L.-M., Yang, B., Ye, C., Xiao, H., Meng, Q.-Y., Ramamurthy, V., Tung, C.-H., and Wu, L.-Z. (2017). General and efficient intermolecular [2+2] photodimerization of chalcones and

cinnamic acid derivatives in solution through visible-light catalysis. Angew. Chem. Int. Ed. *56*, 15407–15410.

62. Shcherbakova, V., Dibchak, D., Snisarenko, M., Skalenko, Y., Denisenko, A.V., Kuznetsova, A.S., and Mykhailiuk, P.K. (2021). Bicyclic piperidines via [2+2] photocycloaddition. J. Org. Chem. *86*, 2200–2209.

63. Kaga, A., Wu, X., Lim, J.Y.J., Hayashi, H., Lu, Y., Yeow, E.K.L., and Chiba, S. (2018). Degenerative xanthate transfer to olefins under visible-light photocatalysis. Beilstein J. Org. Chem. *14*, 3047–3058.

64. Becker, M.R., Wearing, E.R., and Schindler, C.S. (2020). Synthesis of azetidines via visible-light-mediated intermolecular [2+2] photocycloadditions. Nat. Chem. *12*, 898–905.

65. Richardson, A.D., Becker, M.R., and Schindler, C.S. (2020). Synthesis of azetidines by aza Paternò–Büchi reactions. Chem. Sci. *11*, 7553–7561.

66. Tong, S., Li, K., Ouyang, X., Song, R., and Li, J. (2021). Recent advances in the radical-mediated decyanative alkylation of cyano(hetero)arene. Green Synth. Catal. *2*, 145–155.

67. Zhou, C., Lei, T., Wei, X.-Z., Ye, C., Liu, Z., Chen, B., Tung, C.-H., and Wu, L.-Z. (2020). Metal-free, redox-neutral, site-selective access to heteroarylamine via direct radical–radical cross-coupling powered by visible light photocatalysis. J. Am. Chem. Soc. *142*, 16805–16813.

68. The reaction between 47 and 48 in the presence of PIq-10 as the photoredox catalyst (otherwise the same reaction conditions as in Table 7) gave decarboxylative coupling product 49 only in 20% yield along with the C–O coupling product, ester 50, in 60% yield. In this case, the higher triplet-state energy of PIq-10 made sensitization-driven C–O reductive elimination outcompete oxidative decarboxylation.

69. Wearing, E.R., Blackmun, D.E., Becker, M.R., and Schindler, C.S. (2021). 1- and 2-Azetines via visible light-mediated [2 + 2]-cycloadditions of alkynes and oximes. J. Am. Chem. Soc. *143*, 16235–16242.